NUMERICAL SIMULATION OF THE PERFORMANCE OF SAND COLUMNS

By

SATHISHBALAMURUGAN MURUGAIAH

A thesis submitted in partial fulfillment of
the requirements for the degree of

MASTER OF SCIENCE IN CIVIL ENGINEERING

WASHINGTON STATE UNIVERSITY
Department of Civil and Environmental Engineering

December 2004

ACKNOWLEDGEMENT

First and foremost, I would like to express my gratitude to my advisor, Dr. Balasingam Muhunthan. Dr. Muhunthan has guided me in several aspects of my development as a graduate student, not only by giving me the opportunity to pursue exciting and relevant research but also by teaching me how to present my work in a precise and elegant manner. His invaluable knowledge, patience and continuous support made every second of the project immensely gratifying. His dedication and love for research and academic excellence have rubbed off on me. Most of all, he has been a friend and a mentor whenever I needed one.

Special thanks are extended to the Department of Civil and Environmental engineering, Washington State University and to Federal High Ways Administration for the financial support. Their generous support has helped me pursue research in this prestigious university.

I am also indebted to Dr. Adrian Rodriguez-Marek and Dr. Rafik Itani for their time, patience, and suggestions. It was a pleasure working with Dr. Rodriguez-Marek as a teaching assistant, an experience that was invaluable in terms of the knowledge I gained. I am grateful for his constant support and friendship. I would like to thank my friends and colleges for their kindness and cooperation, especially Ilankatharan, Sasiharan, Surendran and Dinesh for their helps in many aspects.

Most Importantly, thanks to my parents Murugaiah and Selvaratnam and sister Balanithy for their love and support. All that I have achieved is because of you.

NUMERICAL SIMULATION OF THE PERFORMANCE OF SAND COLUMNS

Abstract

By Sathishbalamurugan Murugaiah, M. S.

Washington State University

December 2004

Chair: Balasingam Muhunthan

Sand columns have been widely used to improve a range of soils less suitable for other techniques. The installation of sand columns results in the improvement of engineering properties. Current design and performance analysis of sand columns are limited and are mostly empirical. Most analytical methods consider the sand column and the surrounding ground as an elastic composite model and develop equivalent properties.

The effectiveness of compaction and increase in density is dependent on the initial state of soil. Therefore, a state parameter that combines void ratio and mean stress is used here to better characterize the behavior of improved ground. This state parameter is incorporated into a numerical model and used to study the performance of improved ground.

Numerical simulation of the deformation characteristics of an embankment on weak clay reinforced with stone columns was carried out using FLAC 3D. The problem was also analyzed by using equivalent critical state parameters of the composite ground.

The results of the equivalent parameter model were found to correlate well with the analysis of the original configuration.

The numerical analyses show that the improvement in vertical as well as lateral displacement of the embankment is dependent very much on the location and the extent of the placement of sand columns. The displacement patterns of an unimproved ground provide guidance towards the economical placement of the sand columns. The numerical results also show that beyond 40% improved area ratio very little improvement in displacement is achieved.

The study conducted quantified the influence of the initial state of the ground on improved performance. It was found that for a given modular and improved ratios, improvement in vertical displacement ratio could vary significantly depending on the initial state parameter value.

TABLE OF CONTENTS

LIST OF TABLES

LIST OF FIGURES

CHAPTER 1

INTRODUCTION

1.1 Background

Sand columns have been widely used to improve a range of soils from very soft clays and peat to materials less suitable for other techniques. Current environmental constraints often prohibit the use of many other feasible techniques such as preloading, dredging, and soil replacement. In addition, dynamic compaction and blasting are not suitable in urban areas because of their high level of noise and vibration. Sand columns represent an alternative method of ground improvement that has a proven record of performance.

Sand compaction piles are constructed by driving a steel casing filled with sand to the desired elevation using a heavy vertical vibrator placed at the top of the pile. The casing is then gradually extracted using a stroking motion to densify the sand. Using this construction sequence, soft cohesive soils surrounding the sand pile are not left partially unsupported, as is usually the case during the construction of stone columns. Furthermore, sand columns are constructed by dumping sand down the casing and not down an uncased hole as in stone column construction. Since jetting is not normally used, construction of sand columns does not result in a large quantity of excess muddy water that is often environmentally objectionable in stone column construction. Erosion of fines into the sand columns is not a problem for normally used gradations of sand. Finally, construction of sand columns, which is efficient and fast, utilizes low-cost, often locally available sand (Barksdale, 1987).

Even though there are differences in the construction procedures, the mechanical behavior of sand columns and stone columns are essentially the same. The present study is focused on the mechanical properties of the improved ground. Therefore, the terms sand column and stone column are used interchangeably.

Stone columns were first employed in Europe in the 1830's and have been used there extensively since the late 1950's. The practice was adopted in the US since the early 1970's. The results of in-situ soil tests performed before and after sand column installation have shown that soil density can be significantly increased (Aiban, 2002; Ashford et al., 2000; Mitchell, 1981). Installation of sand columns densifies loose deposits. It provides a reinforcing effect, increases the horizontal effective stress and acts as a vertical drain. The use of the sand columns have been identified in different applications of geotechnical engineering such as the reduction in settlements of structures, reduction in earthquake induced liquefaction potential, increased bearing capacity of the foundation and improved stability of slopes. Stone columns have also proven useful in providing drainage and reducing the potential for buildup of excess pore water pressure (Ashford et al., 2000).

Even though sand columns have been use for long, the design is based on empirical or semi analytical approaches (Bachus and Barksdale, 1989). Several researchers have developed equivalent properties of the treated ground using an elastic composite model for the sand columns and the surrounding ground. During the construction of the sand columns the materials undergo plastic deformation. Therefore, as expected the performance of equivalent elastic models have not been satisfactory.

The state of sand and clay and their behavior is controlled by the combined effects of void ratio and mean stress. Therefore, methods to quantify the performance of sand columns on weak soils must take their state into account. The critical state line provides a convenient reference datum to study the combined effects of state (Schofield and Wroth 1968). This study develops a state parameter model for the composite behavior of sand columns and weak soil and uses it in the numerical analyses using a finite difference code.

1.2 Objectives

The specific objectives of the study are to:

(i) develop a state based approach to capture the behavior of soft soils improved with sand columns,

(ii) numerically simulate the behavior of improved ground using the original arrangement of columns and by using equivalent state properties, and

(iii) compare results with performance from past field studies.

The study makes use of the finite difference code FLAC 3D developed by Itasca. The focus of the study is on the reduction of settlement in embankments constructed on weak soils using stone columns. The methodology used, however, is applicable for any other boundary value problem in geotechnical engineering.

1.3 Organization of Thesis

This thesis organized in to six chapters. Chapter 2 provides a literature review of the current models used to quantify the performance of stone columns on weak soils.

Chapter 3 presents the theoretical background of the state concept and the equivalent state parameter model for the composite improved ground consisting of sand columns and weak soils. A brief description of the constitutive models used in the FLAC 3D analysis is provided in Chapter 4. The numerical analyses of the settlement characteristics of the embankment are presented in Chapter 5. The FLAC 3D model is first verified on a field test embankment and then used to study the effects of improving the weak ground using sand columns. This chapter also provides a parametric study of the influence of the key variables that affect the performance of improved ground including the state of soil. The sixth and final chapter presents a summary of the major conclusions reached from this study and makes recommendations for future research in this area.

CHAPTER 2

LITERATURE REVIEW

Many analytical and numerical studies have been conducted to develop design guidelines for sand columns. Since the improved ground consists of sand columns and the surrounding soil most analytical studies have used some type of homogenization technique to derive equivalent homogenized properties for the improved ground based on the properties of the individual constituents. The numerical studies have consisted mainly of finite element analyses.

2.1 Analytical Models

2.1.1 Poorooshasb and Meyerhof (1997)

Fig. 2.1 shows the plan and cross-sectional views of an end bearing series of stone columns installed in a weak soil to reduce the settlement of a raft foundation system. The system can be idealized as consisting of a uniform distributed load, UDL, spread over the column spacing 2b. The equilibrium of the forces in the vertical direction requires that (Fig. 2.1 (c)):

$$\mathrm{UDL} = \frac{a^2\sigma_1 + (b^2 - a^2)\,p}{b^2} \qquad (2\text{-}1)$$

where σ_1 is the maximum principal stress, p is the load intensity carried by the weak soil and a is the radius of stone column.

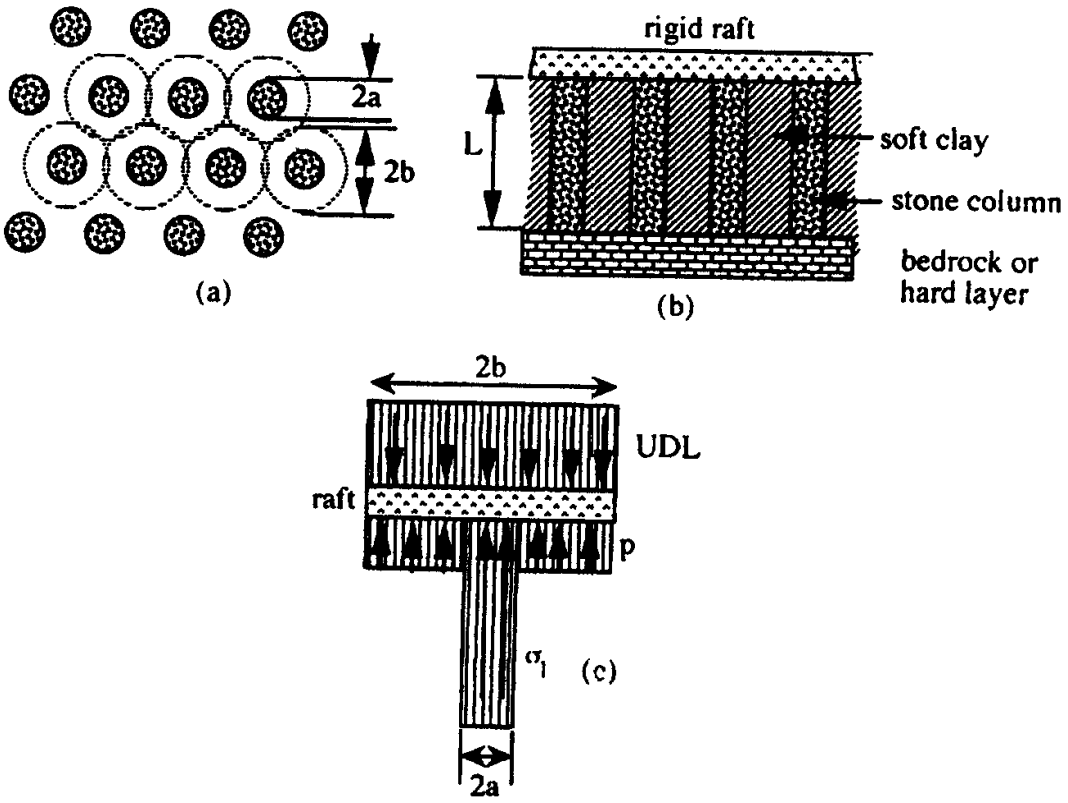

Fig. 2.1: Stone column arrangement and the equivalent model (Poorooshasb and Meyerhof, 1997)

For columns with a linear elastic material with a Young's modulus E_c and a Poisson's ratio of ν_c, it can be shown that:

$$\frac{UDL}{\delta/L} = A\{1 + B\nu_c\}\frac{b^2 - a^2}{b^2} + \{E_c + 2\nu_c[AC(1 + B\nu_c) + D\nu_c]\}\frac{a^2}{b^2} \qquad (2\text{-}2)$$

where L is the height of the column, δ is the settlement and the constants A, B, C and D are given by (Poorooshasb an Meyerhof 1997):

$$A = \frac{(1-\nu)}{1 - 2\nu^2 - \nu}E_s \qquad (2\text{-}3)$$

$$B = \frac{2\nu}{1-\nu}\frac{a^2}{b^2 - a^2} \qquad (2\text{-}4)$$

$$C = \frac{\nu}{1-\nu} \tag{2-5}$$

$$D = \frac{(1+\nu)a^2 + (1-\nu)b^2}{(1-\nu^2)(b^2-a^2)} E_s \tag{2-6}$$

where ν is the Poisson's ratio of the in situ soil and E_s is its Young's modulus. Note that if $\nu_c = 0$ and $\nu = 0$ then $A = E_s$ and $B = 0$, then Eq. 2-2 reduces to:

$$n = \frac{(UDL/E_s)}{(\delta/L)} = 1 + A_r\left(\frac{E_c}{E_s} - 1\right) \tag{2-7}$$

In Eq. 2-7 n is the settlement ratio and A_r is the area ratio and represents the area of cross section of the column to the area of the cross section of the influence cell (a^2/b^2) (Priebe, 1976).

The performance ratio, PR, of the system is defined as the ratio of the settlement of the improved ground to that unimproved ground under identical surcharges. Thus the relation between performance ratio and the settlement ratio can be stated as:

$$PR = 1/n = \frac{\delta}{L}\frac{E_s}{UDL} \tag{2-8}$$

PR was found to depend on the spacing, s, internal angle of friction of the column material, φ, and the failure strain of column material, ε_f (Poorooshasb and Meyerhof, 1987). Consequently, sets of design charts were developed as shown in Fig. 2.2. Since these charts were developed based on the assumption of a zero Poisson's ratio for the soft soil, they may be used to get a conservative estimate of PR. For other conditions Eq. (2-8) can be modified as:

$$PR = \frac{\delta}{L}\frac{E'}{UDL} \tag{2-9}$$

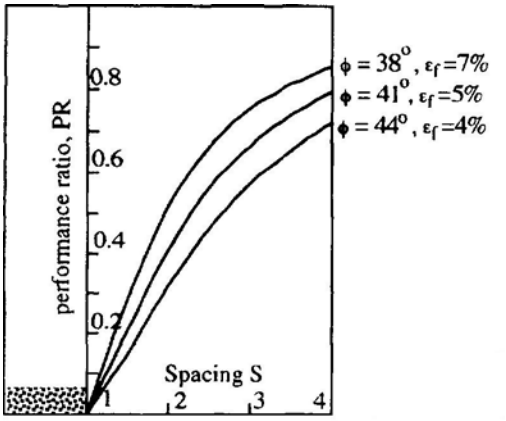

(a)

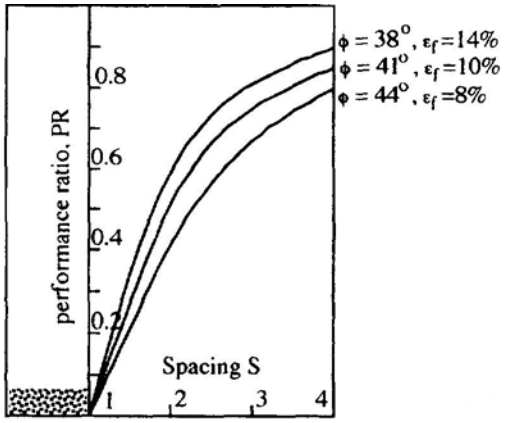

(b)

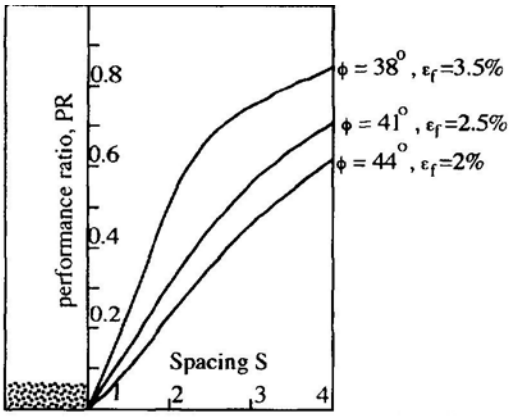

(c)

Fig. 2.2: Performance ratio vs. Spacing for (a) Standard stone columns (b) Stone columns less stiff than standard (c) Floating stone columns stiffer than standard.

where E′ is the modified Young's modulus for the soft soil corrected for the Poisson's ratio effect, given by:

$$E' = \frac{1-\nu}{1-\nu-2\nu^2} E_s \tag{2-10}$$

2.1.2 Omine and Bolton (1998)

Omine and Bolton (1998) proposed an approach to predict the stress-strain relationship of sand - clay mixtures in a stone column arrangement using the homogenization theory proposed by Eshelby (1957). Eshelby pointed out that the stress disturbance in an applied stress due to the presence of an inhomogeneity could be simulated by the eigenstress caused by the inclusion with a proper choice of the eigenstrain.

Fig. 2.3 shows the schematic diagram of the stone columns and the in situ soil. In order to evaluate stress distribution within the mixture, a stress distribution tensor, b_{ijkl}, which represents relationship between the stresses of inclusion and the matrix, is introduced. The stress distribution tensor b_{ijkl} is dependent on the shape and the orientation of the stress tensor of the inclusion. The stress distribution tensor of the mixture with elliptical and cylindrical inclusions laminated in the direction of the stress tensor can be defined as:

$$b = \left(\frac{E_s}{E^*} \right)^{1-S_{iiii}} \tag{2-11}$$

where E_s is the Young's Modulus of the inclusion, E* is the Young's modulus of the matrix and S_{iiii} is the Eshelby tensor. Note that for simplicity the subscripts in b are

omitted. For vertical inclusion with a stress applied only in the vertical direction $S_{iiii} = 0$ (Omine and Bolton, 1998). Accordingly Eq. 2-11 reduces to:

$$b = \left(\frac{E_s}{E^*} \right) \tag{2-12}$$

furthermore, for the condition of non-zero vertical stress with all other stresses being zero, the equivalent Young's modulus of the mixture can be represented by (Omine and Bolton, 1998):

$$E = \frac{(b-1) f_s + 1}{\frac{f_s b}{E_s} + \frac{(1-f_s)}{E^*}} \tag{2-13}$$

where f_s is the volume fraction of the inclusions.

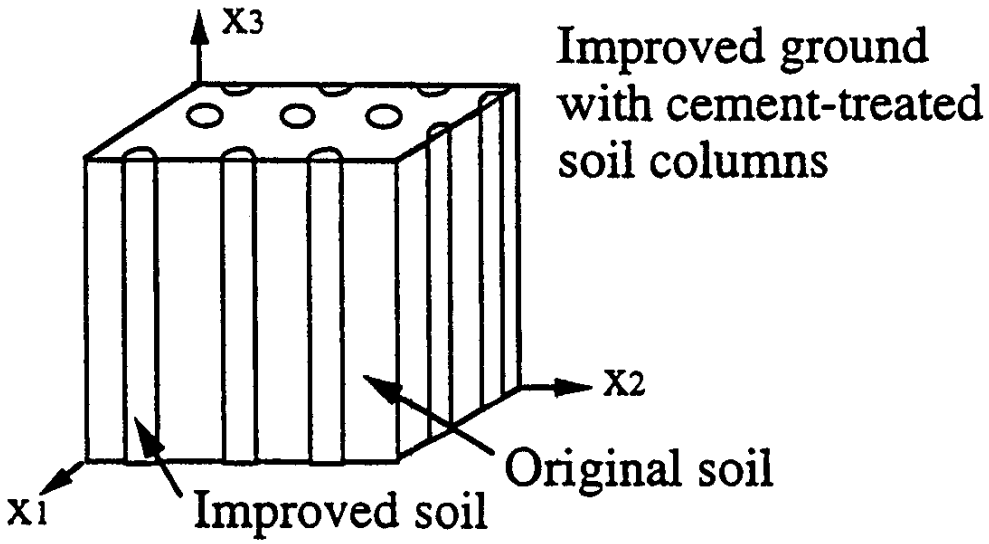

Fig. 2.3: Sand-clay mixture in improved ground (Omine and Bolton, 1998).

The above homogenization technique is useful for a mixture with extremely different stiffness of the basic material and inclusion. Since the interaction among inclusion increases as the volume content of inclusions increases, the application of this method is also limited to mixtures with a small content of inclusions.

2.1.3 Wang, Leung, and Ichikawa (2002)

Fig. 2.4 shows the schematic diagram of stiff soil columns within a soft soil system. This system was considered as a unit composite cell consisting of the matrix material (termed m-phase) and the reinforcement material (termed f-phase). The stress ratio, b_s, between the two materials is defined as:

$$b_s = \sqrt{\frac{E_f}{E_m}} \tag{2-14}$$

where E_f is the Young modulus of the inclusion and E_m is the Young modulus of the matrix.

Based on the assumption that the stress in each phase of a unit cell is homogeneous and that the stresses in the different phases are distributed according to their proportion, a localization tensor C is developed as:

$$\mathbf{C}=\begin{Bmatrix} \dfrac{b_s}{(b_s-1)f_s+1}\mathbf{I} \\ \dfrac{1}{(b_s-1)f_s+1}\mathbf{I} \end{Bmatrix} \begin{matrix} \text{in f}-\text{phase (inclusion)} \\ \text{in m}-\text{phase (matrix)} \end{matrix} \tag{2-15}$$

where b_s is the stress ratio, f_s is the volume fraction of the inclusion and **I** is a fourth order unit tensor. The localization parameter **C** is used to predict other equivalent characteristics such as the Young's Modulus and strength of the composite medium.

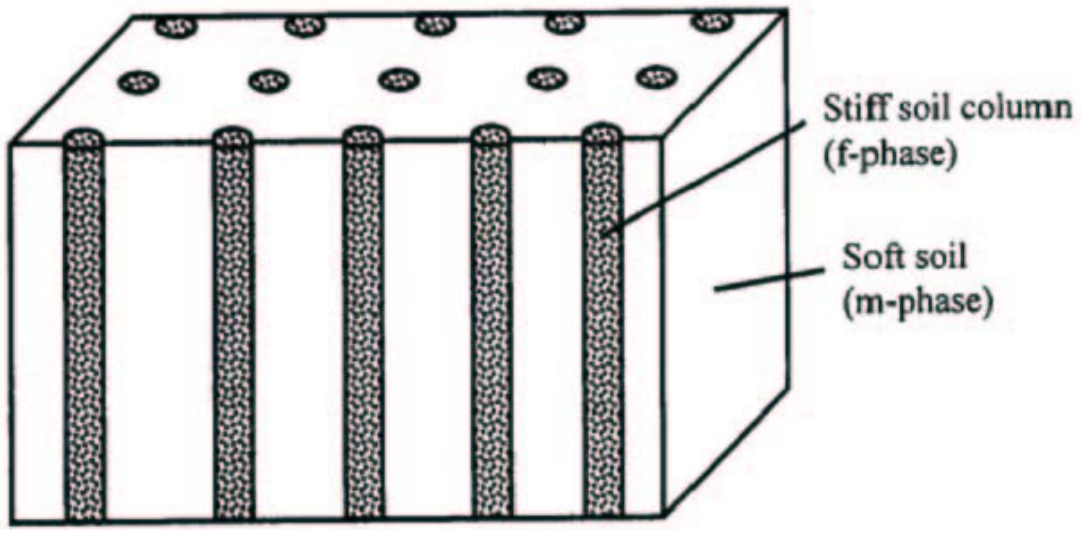

Fig. 2.4: Soft soil improved with stone columns (Wang et al., 2002)

Composite ground consists of improved and unimproved parts because stiff soil is installed as columns and does not mix with the in-situ original soil outside the stiff soil columns and the reinforcement has definite orientation in space. Micro-stress is again assumed to be homogeneous in improved and unimproved parts. Since the micro stress is distributed according to the stress localization tensor **C**, the micro-stress at the failure for the reinforcement phase and matrix phase can be determined to be:

$$q'_{uf} = \frac{b_s}{(b_s - 1)f_s + 1} q_{uf} \tag{2-16}$$

$$q'_{um} = \frac{1}{(b_s - 1)f_s + 1} q_{um} \tag{2-17}$$

where q_{uf} and q_{um} are macro stress at failure for reinforcement phase and matrix phase respectively. Consequently, the homogenized strength q_u^h is established as follows:

$$q_u^h = f_s q'_{uf} + (1 - f_s) q'_{um} = \frac{b_s f_s q_{uf} + (1 - f_s) q_{um}}{(b_s - 1) f_s + 1} \quad (2\text{-}18)$$

Since the micro strain in the vertical direction should be the same for each phase and equal to the macro strain, the homogenized deformation modulus E_{50}^h can be obtained by dividing the homogenized strength by macro strain:

$$E_{50}^h = \frac{b_s f_s E_{50f} + (1 - f_s) E_{50m}}{(b_s - 1) f_s + 1} \quad (2\text{-}19)$$

2.1.4 Evaluation of homogenized models

A typical problem of an end bearing stone columns with a radius of 0.5 m installed in an in situ soil was considered to evaluate the performance of the different homogenized models. Fig. 2.5 shows the arrangement of the columns in an in situ soil. Stone columns with a stiffer material having a Young's modulus of 15,000kPa and range of Poisson's ratio from 0.2 to 0.49 were constructed within the soil with a Young's modulus of 1,000kP and a Poisson's ratio of 0.2. The elastic moduli of the improved ground were calculated for different column spacings. The heights of the columns are assumed to be equal to the thickness of the soil layer.

The equivalent Young's modulus of the composite ground was calculated using the different approaches previously discussed and plotted with the spacing of the columns as shown in Fig. 2.6. It can be seen that with increased spacing the equivalent modulus decreases. The results of Poorooshasb and Meyerhof (1997) and Omine and Bolton (1998) correlate well. However, the method of Wang et al., (2002) produced higher Young's modulus values for the same spacing.

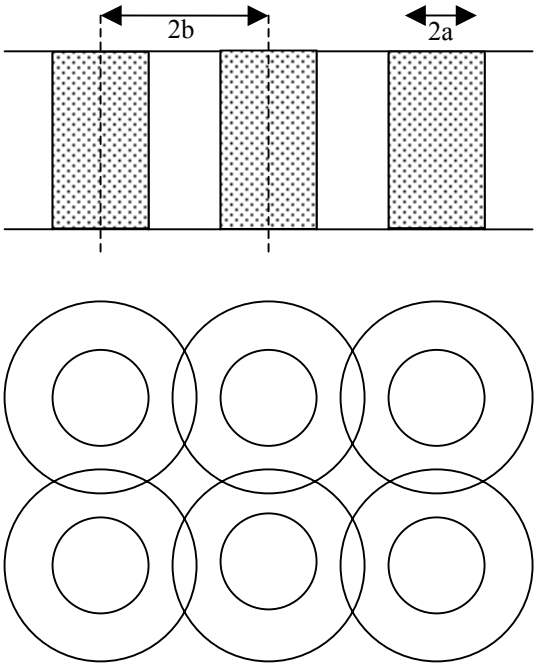

Fig. 2.5: Model used in typical problem

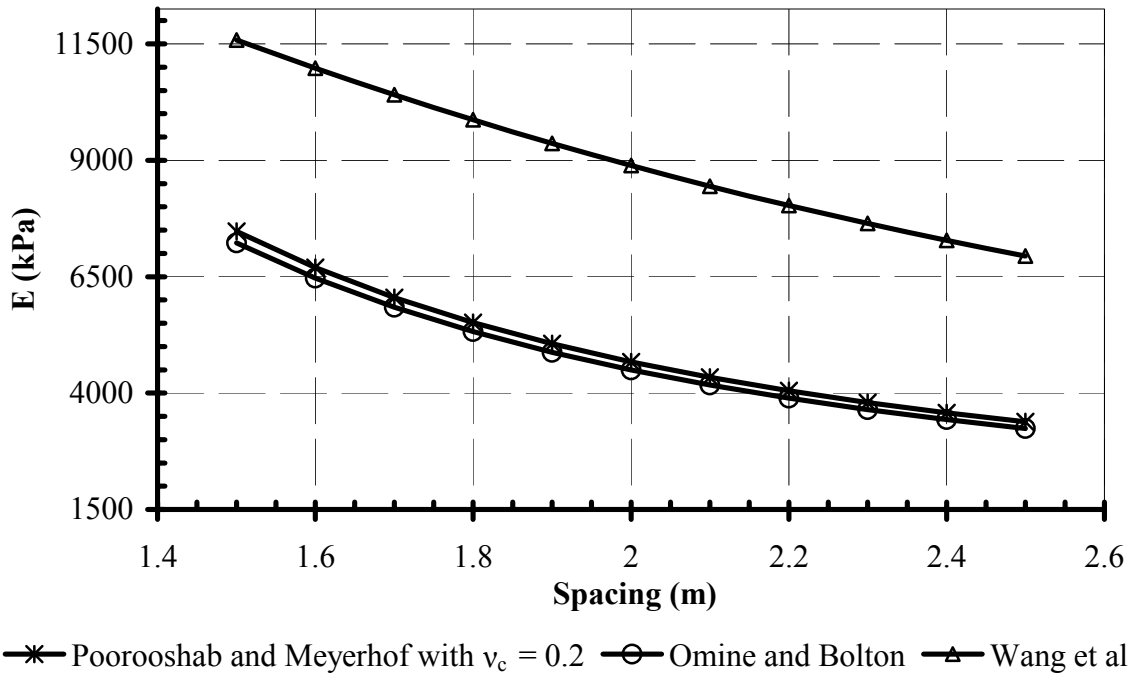

Fig. 2.6: Variation of equivalent Young's modulus with spacing of columns

2.1.5 Improvement factor

Priebe (1995) proposed an improvement factor that could be used to assess the performance of stone columns. In this case a unit cell with area A is considered consisting of a single column with the cross section A_c and the attributable surrounding soil. The calculation of the basic improvement factor was done by considering the stone columns to be incompressible material installed within a rigid layer. The bulk densities of column and soil also were neglected. Hence, the column cannot fail in end bearing and any settlement of the load area results in a bulging of the column which remains constant all over its length.

The improvement of a soil achieved by the presence of stone columns is evaluated based on the assumption that the column material shears from the beginning whilst the surrounding soil reacts elastically. Furthermore, the soil is assumed to be displaced already during the column installation to such an extent that its initial resistance corresponds to the liquid state: i.e. the coefficient of earth pressure amounts to K=1. The result of the evaluation produces the basic improvement factor as a function of A_c, A, Poisson's ratio μ_s, and the friction angle φ_c. Since a Poisson's ratio of 1/3 is adequate for the state of final settlement in most cases, substituting 1/3 for the Poisson's ratio the basic improvement factor was defined as (Priebe, 1995):

$$n_0 = 1 + \frac{A_c}{A}\left[\frac{5 - A_c/A}{4K_{ac}(1 - A_c/A)} - 1\right] \tag{2-20}$$

where,

$$K_{ac} = \tan^2(45 - \varphi_c/2) \tag{2-21}$$

and φ_c is the friction angle of the stone column material.

The variation of the basic improvement factor n_0 with the reciprocal area ratio can be plotted for different friction angles of backfill material as in Fig. 2.7.

The compressibility effect of the columns was incorporated by adding up an additional area ratio as a function of the constrained modulus of the column, D_c and that of the surrounding soil, D_s. Fig. 2.8 provides the additional area ratio necessary for different constrained modulus ratio (D_c/D_s) and friction angle of the column material. The additional loads due to the bulk densities of the soil and columns decrease the pressure difference asymptotically and reduce the bulging correspondingly. Consequently, multiplying the basic improvement factor by a depth factor could incorporate the effect of the bulk density. The depth factor is given by:

$$f_d = \frac{1}{\left[1 - y.\sum(\gamma_s.\Delta d)/p\right]} \tag{2-22}$$

where f_d - depth factor,

y - influence factor

γ_s – bulk density of the soil

Δd – layer thickness

p – area load respective to foundation

The influence factor y as a function of the Area ratio is given in Fig. 2.9. Note that the above relationship was developed by assuming the bulk density of the columns and the soil to be equal. This, however, may not be true in most cases. Therefore, to be on the safer side, Priebe suggested the use of lower values of bulk density in the calculations. The final improvement factor n_2 is defined as:

$$n_2 = f_d n_1 \tag{2-23}$$

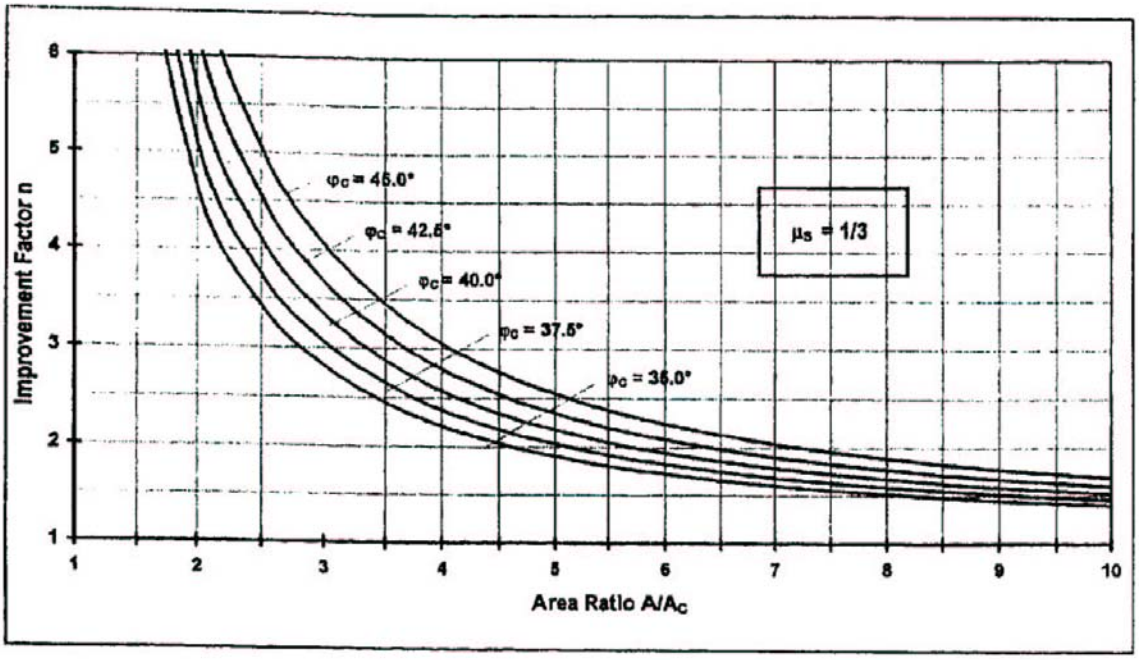

Fig. 2.7: Improvement factor vs. Area ratio (Priebe, 1995)

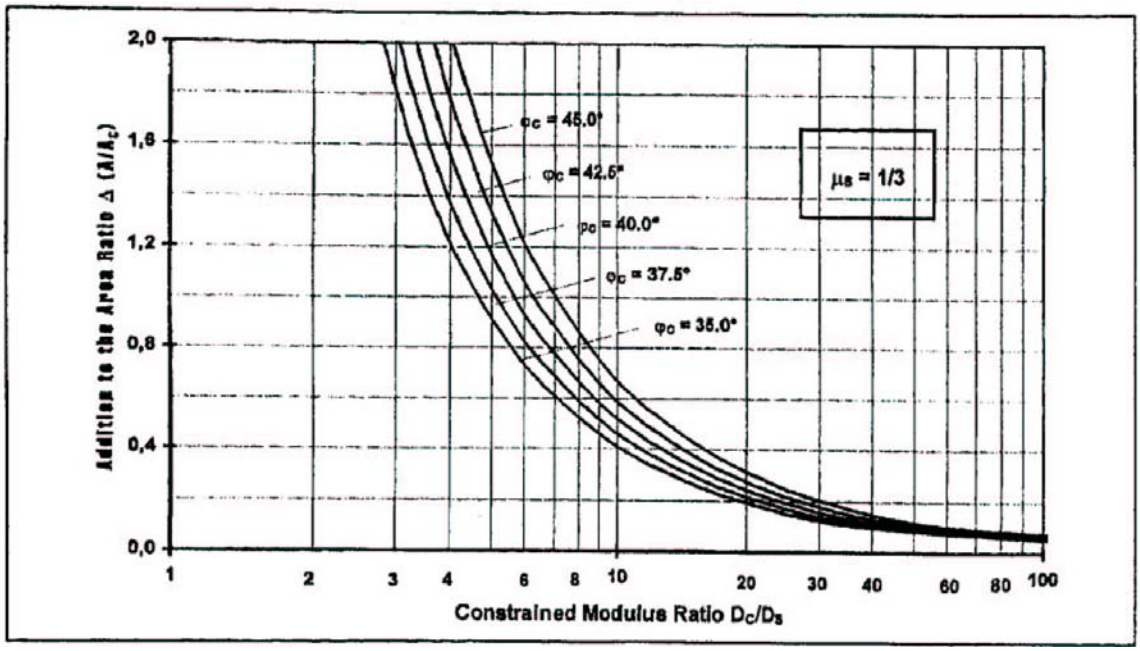

Fig. 2.8: Addition to the area ratio vs. constrained modulus ratio (Priebe, 1995)

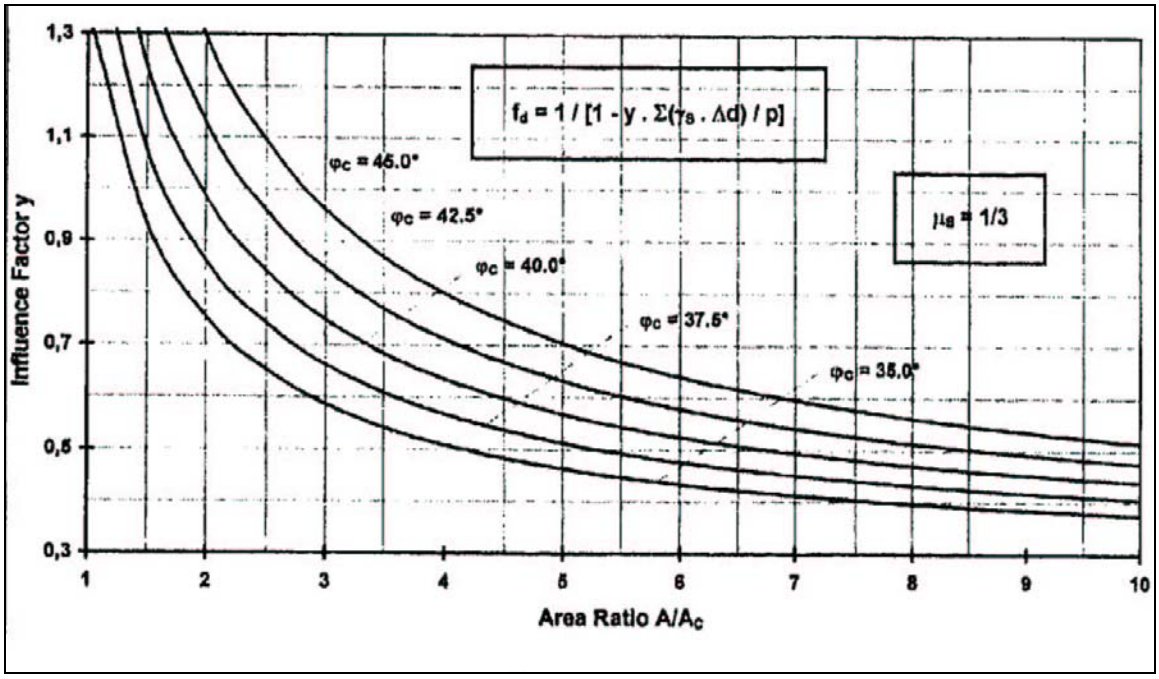

Fig. 2.9: Influence factor vs. Area ratio (Priebe, 1995)

2.1.6 Alamgir, Miura, Poorooshasb, and Madhav, (1996)

A theoretical approach based on the deformation properties of the column material and the surrounding soil was developed by Alamgir et al., (1996) to predict the deformation behavior of a foundation system on an improved ground (Fig. 2.10). The deformation across a cross section within the column, w_{cz}, is assumed to be constant and the deformation of the surrounding soil, w_{rz}, is assumed to increase from the soil column interface towards the boundary of the unit cell (Fig. 2.11). Note that this assumes that the column-soil interface remains elastic and no slip occurs, the displacements of the column and the soil at the interface can be assumed to be equal.

The column and the surrounding soil were discretized in to a number of elements as shown in Fig. 2.12. The deformation of the surrounding soil, w_{rz}, is assumed to follow:

$$w_{rz} = w_{cz} + \alpha_{cz}\left[r/a - e^{\beta_c(r/a-1)}\right] \quad \text{for} \quad a \le r \le b \tag{2-24}$$

where a and b are the radii of column and unit cell, respectively, r is the radial distance measured from the center of the column, w_{rz} is the displacement of the soil element at a depth z and at a radial distance r, w_{cz} is the displacement of the column element at a depth z, α_{cz} and β_c are the displacement parameters.

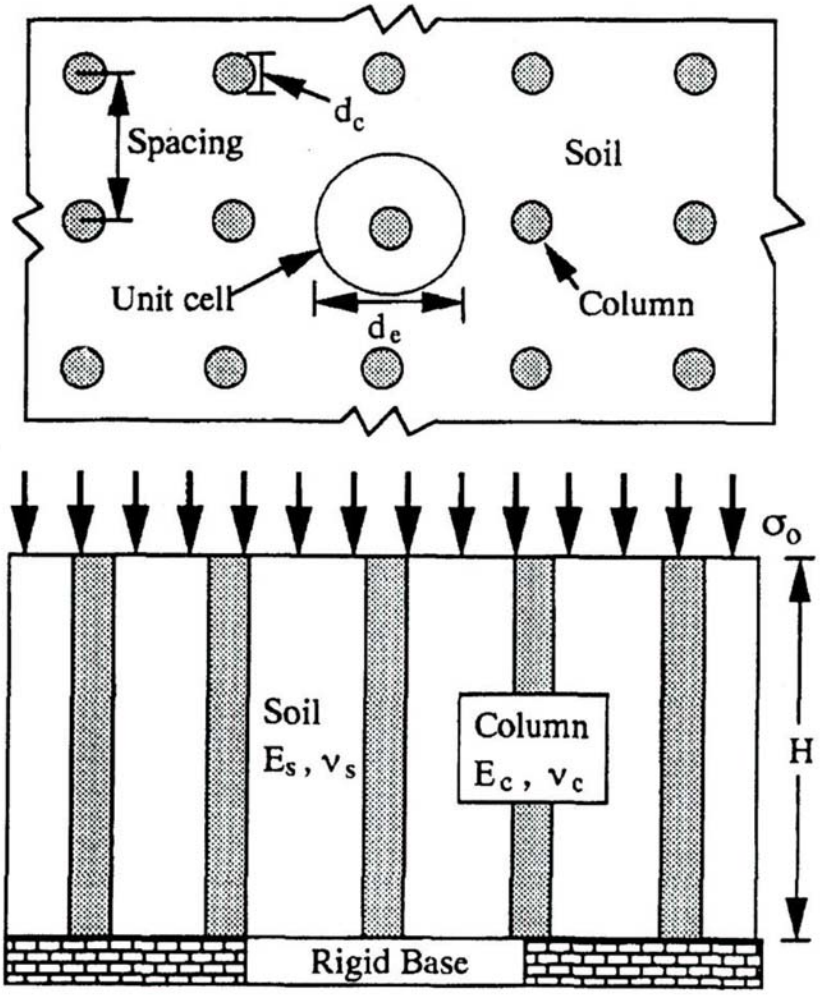

Fig. 2.10: Foundation system on an improved ground (Alamgir et al., 1996)

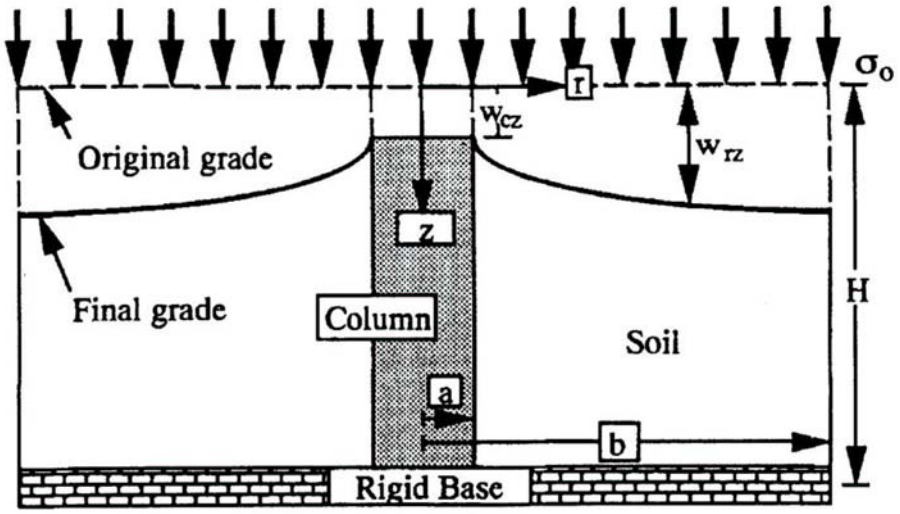

Fig. 2.11: Unit cell and the assumed mode of deformation (Alamgir et al., 1996)

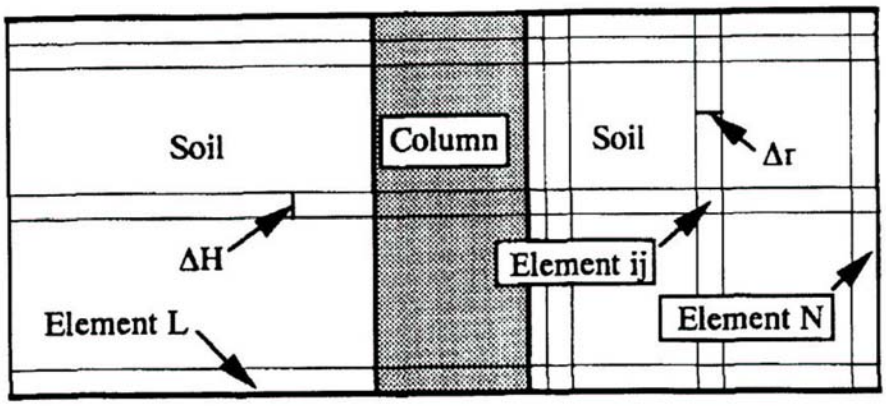

Fig. 2.12: Discretization of the surrounding soil (Alamgir et al., 1996)

The equilibrium of vertical forces within the medium was considered to obtain the interaction shear stresses and stresses on the column and the soil. Subsequently, the equations were solved by applying elastic deformation characteristics of the column and soil to obtain the displacements of columns and soil. Accordingly, the deformation of the j^{th} element of the column (Fig. 2.10), w_{cj} was determined as:

$$w_{cj} = \frac{\Delta H}{E_c}\sigma_{cj} + \frac{(\Delta H/a)^2\left(1-\beta_c\right)E_s\alpha_{cj}}{2E_c\left(1+\upsilon_s\right)} \qquad (2\text{-}25)$$

where ΔH is the height of a single element, E_c and E_s are the modulus of deformations of column material and soil respectively, σ_{cj} is the normal stress acting at the top of the j^{th} element of the column and υ_s is the Poisson's ratio of the soil.

The compression of the soil element adjacent to the boundary of unit cell w_{sNj} was derived as:

$$w_{sNj} = \frac{\Delta H}{E_s}\sigma_{sNj} - \frac{(\Delta H/a)^2 (n - \Delta R)\left[1 - \beta_c e^{\beta_c((n - \Delta R - 1)}\right]\alpha_{cj}}{4\Delta R(n - \Delta R/2)(1 + \upsilon_s)} \qquad (2\text{-}26)$$

where σ_{sNj} is the normal stress acting at the top of the element, n is the spacing ratio b/a ΔR is $\Delta r/a$ and Δr is (b-a)/n.

By using the displacement compatibility and substituting r/a=n- $\Delta R/2$ Eq. 2-24 can be written as

$$w_{sNj} = w_{cj} + \alpha_{cj}\left[n - \Delta R/2 - e^{\beta_c(n - \Delta R/2 - 1)}\right] \quad \text{for} \quad a \le r \le b \qquad (2\text{-}27)$$

Due to the symmetry of the loading geometry the shear stress at the outside boundary of the unit cell is zero and that leads to an equation for β_c as:

$$\beta_c e^{\beta_c(n-1)} - 1 = 0 \qquad (2\text{-}28)$$

From Eqs. 2-25, 2-26, 2-27 and 2-28, the displacement parameter α_{cj} could be calculated. This leads to assume a simplified deformation pattern for an in situ soil improved with stone columns. Distribution of shear stresses, the stresses on the columns and in situ soil and the stress concentration ratio can be estimated using the assumed deformation pattern.

2.2 Numerical analysis

2.2.1 Kirsch and Sondermann (2003)

Kirsch and Sondermann (2003) used a 3-D finite element analysis to study the settlement pattern and shear stress distribution on an embankment reinforced with stone columns (Fig. 2.10). Isoparametric brick elements with square interpolation functions and three degrees of freedom at each node were used to discretize the embankment. The Drucker-Prager yield criterion (Drucker and Prager, 1952) with a non-associated flow rule was employed in the simulation. The discretized FE model as well as the stress distribution obtained is as shown in Fig. 2.13.

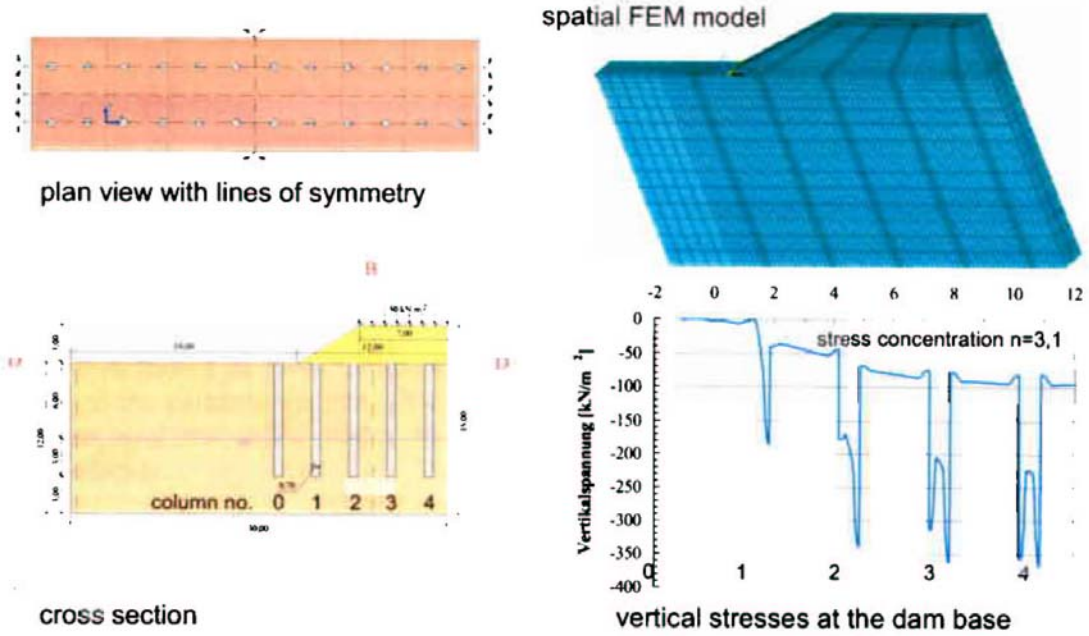

Fig. 2.13: Summary of the numerical analysis (Kirsch and Sondermann, 2003)

Numerical analyses can account for the correct reproduction of the stress distribution between stone columns and surrounding in situ soil. Useful conclusions on approximate factors of safety and failure mechanisms can be drawn form the results of the numerical simulations. Comparisons of the results from both numerical and

analytical computations can lead to a practical approach to study the performance of the stone columns.

2.3 Summary

There has been limited number of analytical methods developed to study the problem of sand column-soil interaction. Most of these approaches considered the soil and column material as elastic. They have also focused the attention on the settlement in the vertical direction. The horizontal displacements play a critical role in many field problems. Therefore, they must also be considered in embankments on soft soils.

Numerical models offer the flexibility to account for many of the variables that control the performance of sand columns. This study will be based on a three dimensional analysis of sand columns in a soft clay media. It considers the improvement on both vertical and horizontal deformations due to the sand columns. It also considers a composite model that can better simulate the actual model based on a state mechanical approach. A set of design charts is developed as part of a parametric study, incorporating the variation of different material properties of soil and column material.

CHAPTER 3

STATE OF SOIL

3.1 Critical state

When a soil or granular medium is continuously sheared, it will ultimately attain a state termed the critical state (Schofield and Wroth, 1968). At the critical state, soil continuously shears as a frictional fluid with no further changes in stress or volume. The critical state is generally defined in a three dimensional mean effective stress, deviator stress and specific volume (p′, q, v) space, where

the mean normal effective stress, p′, is defined by:

$$p' = \frac{1}{3}\left(\sigma'_1 + \sigma'_2 + \sigma'_3\right) \tag{3-1}$$

and the deviator stress, q, by:

$$q = \frac{1}{\sqrt{2}}\left(\left(\sigma'_2 - \sigma'_3\right)^2 + \left(\sigma'_3 - \sigma'_1\right)^2 + \left(\sigma'_1 - \sigma'_2\right)^2\right)^{\frac{1}{2}} \tag{3-2}$$

σ_1', σ_2', σ_3' are the principal effective stresses. For a triaxial compression test conditions, $\sigma_2' = \sigma_3'$, and Eqs.3-1 and 3-2 reduce to:

$$p' = \frac{1}{3}\left(\sigma'_1 + 2\sigma'_3\right) \tag{3-3}$$

$$q = \sigma'_1 - \sigma'_3 \tag{3-4}$$

The specific volume v is defined by:

$$v = 1 + e \tag{3-5}$$

The critical state line in the 3-D (p′, q, v) space is as shown in Fig. 3.1. The projection of the CS line on the q, p′ plane is a straight line with slope M whereas the

projection on the v, lnp′ plane is a straight line with slope λ (Fig. 3.2). These projections of the critical state line can be expressed by:

$$q = Mp' \tag{3-6}$$

$$v = \Gamma - \lambda \ln p' \tag{3-7}$$

where Γ is the intercept at p′ = 1 kPa in the v-lnp′ diagram (Fig. 3.2).

The critical state line can be considered as one of a family of parallel compression lines of the form:

$$v_\lambda = v + \lambda \ln p' \tag{3-8}$$

Note $v_\lambda = \Gamma$ at the critical state and $v_\lambda = N_0$ at the isotropic compression line (ICL) (Fig. 3.2). The normal compression line has $v_\lambda = N$.

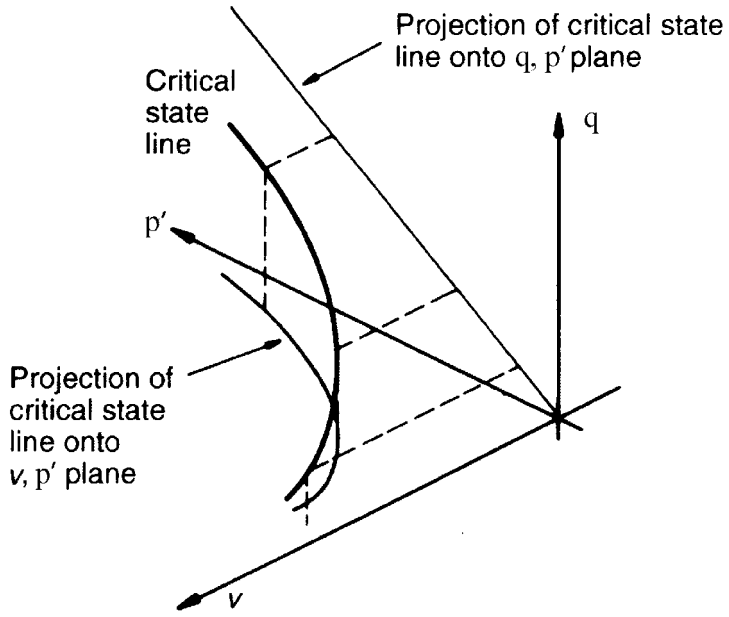

Fig. 3.1: The Critical state line in q, p and v space.

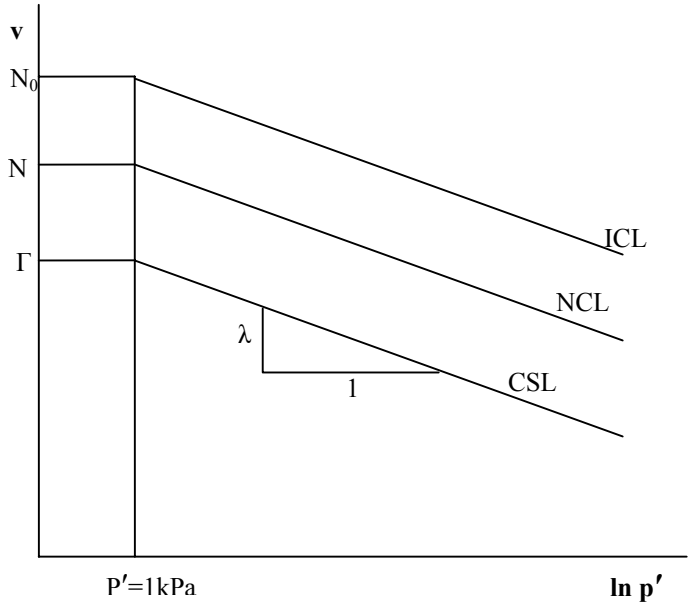

Fig. 3.2: Compression lines in v, lnp′ space**.**

Elastic compression and swelling of soil specimens in general follow lines:

$$v_{\kappa} = v + \kappa \ln p' = \text{const} \tag{3-9}$$

where v_κ is the value of the intercept of any specific line with the v axis and κ is the elastic compressibility. The value of v_κ combines pressure p′ and specific volume v to define the aggregate of grains which corresponds to a specific compression line.

When there is no slip among the grains the aggregate experiences purely elastic changes. Any slippage results in small plastic deformation of the whole aggregate with changes of many contacts between grains. Each time there is plastic deformation a new aggregation of particles is formed, which has a swelling and compression line with the same slope but a different intercept (Muhunthan and Schofield, 2000). A shift between lines indicates a plastic volume change from one aggregation to the next. For illustrative purpose a plot of v_κ against ln p′ (Fig. 3.3 (b)) gives a clearer view of the shift of the

lines. Note that the line of critical states in this plot has slope (λ-κ) (Muhunthan and Schofield, 2000).

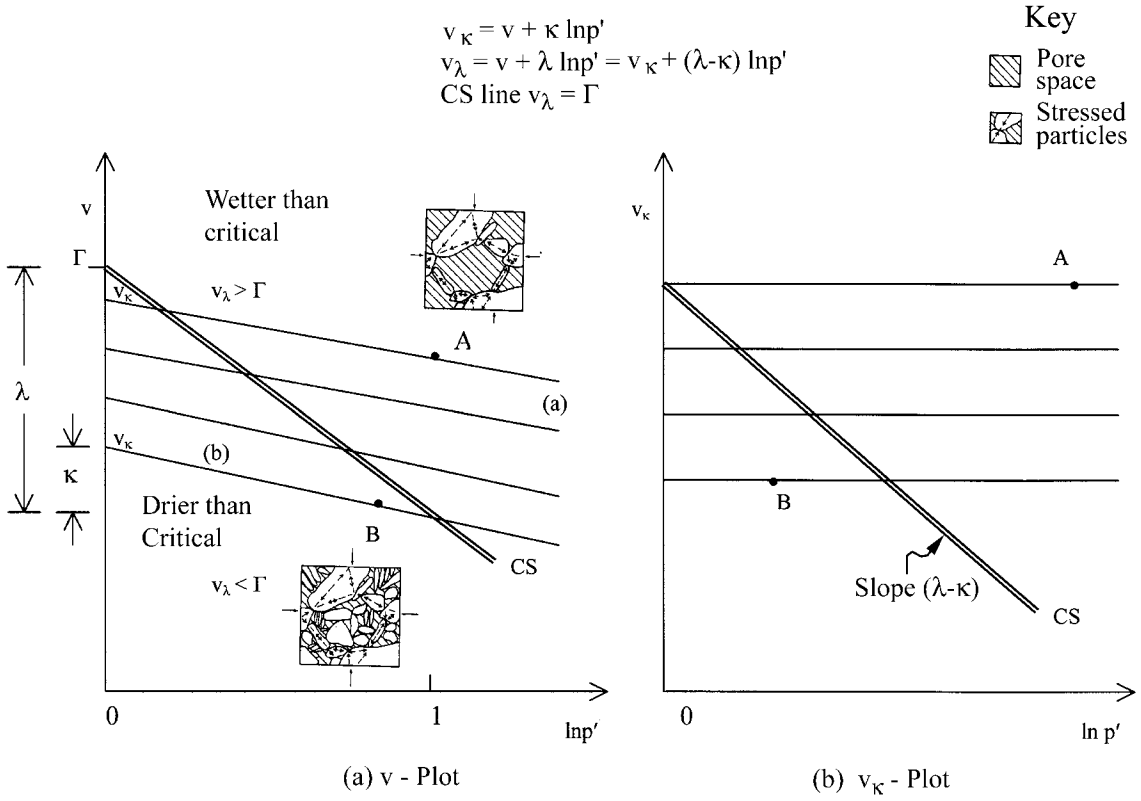

Fig. 3.3: Aggregate behavior and critical states (Muhunthan and Schofield, 2000)

Consider two specimens with aggregates of grains at the same mean normal effective stress on lines (A) and (B) with identical lattices of highly loaded grains, but with different amount of lightly loaded grains (Fig. 3.3(a)). If line (A) has a higher value of v_κ than line (B), then specimen (A) has fewer lightly loaded grains than specimen (B). If we now impose shear stresses on the aggregations represented by (A) and (B) and permit drainage of pore fluid, we may expect slippage of highly loaded particles and plastic volume change. This leads to other grains forming a highly loaded lattice.

The plastic volumetric response of the two specimens at the same mean effective stress will differ depending on the nature of packing of the lightly loaded grains. A specimen on line (A) with fewer lightly loaded grains loosely packed will compact with a fall in v_κ and the dense one on line (B) will dilate with increase in v_κ during plastic shear distortion. Between these two limits there will be a density of packing at which during shear distortion a succession of load carrying skeleton lattices of stressed grains will form and collapse with successive new structures being formed at about the same density of packing. In this shear strain increment a certain proportion of the grains which at one time formed the load carrying skeleton, now as individual grains become relatively lightly stressed or unstressed and play the role of "filler" particles filling voids. The notion of a critical state is that there exists one certain critical packing of grains or critical void ratio, at which continuous flow is possible at constant mean normal effective stress p', without damage to the grains, only with change of positions (Muhunthan and Schofield, 2000).

3.2 State of a soil

The critical state line can be used to distinguish two different classes of behavior of soils. There are states for which the combinations of specific volume v and mean normal effective stress p' lie further away from the origin than the line of critical states, so that,

$$v + \lambda \ln p' > \Gamma , \quad \text{or} \quad v_k + (\lambda - \kappa) \ln p' > \Gamma , \quad \text{or} \quad v_\lambda > \Gamma \qquad (3\text{–}10)$$

and these states have been called "wetter than critical"; under such conditions shearing causes aggregates to compress to more dense packing and emit water with ductile stable

yielding of a test specimen. There are also states of specific volume v and mean normal effective stress p′ such that:

$$v + \lambda \ln p' < \Gamma , \qquad \text{or} \qquad v_k + (\lambda - \kappa) \ln p' < \Gamma , \quad \text{or} \qquad v_\lambda < \Gamma \qquad (3\text{-}11)$$

and these states have been called “drier than critical”; where shearing causes aggregates to dilate and suck in water and ground slips at peak strength with unstable failures.

The distance of the initial state from the critical line is then a measure of the state of the soil that includes both the current stress and the current volume. This distance may be described either in terms of a stress state parameter S_s or by volume state parameter S_v (Atkinson, 1993).

For the state A in Fig. 3.4 these are given by:

$$S_s = p'_a / p'_c \qquad \text{or} \qquad \ln S_s = \ln p'_a - \ln p'_c \qquad (3\text{-}12)$$

$$S_v = \upsilon_a - \upsilon_c \qquad (3\text{-}13)$$

Since the critical line and the normal compression line have the same gradient, the state parameters are related by $S_v = \lambda \ln S_s$, and so either may be used to describe the initial state of the soil. If the state is on the critical state line, $S_v = \ln S_s = 0$; if the state is on the dry side, S_v and $\ln S_s$ are positive. It can be noticed that the stress state parameter S_s is similar to the reciprocal of the over consolidation ratio R_p, but it relates the current state to the critical line rather than to the normal compression line. The volume state parameter S_v is similar to the state parameter defined by Been and Jefferies (1985).

The state parameter has since become an effective mean of characterizing the combined effects of mean stress and void ratio on soil behavior. Pillai and Muhunthan (2001) have shown that the soil capacity in terms of normalized shear strength is a function of the state parameter under undrained monotonic loading as well as cyclic

loading. It was also found that the state parameter in terms of stress ratio (S_s) was a better aid to interpret their results rather than the volume measure. Klotz and Coop (2001) in their investigation on the capacity of the driven piles in sand also concluded that a state parameter defined in terms of a volume difference did not work for sands and that the state needed to be quantified in terms of ratio of stresses.

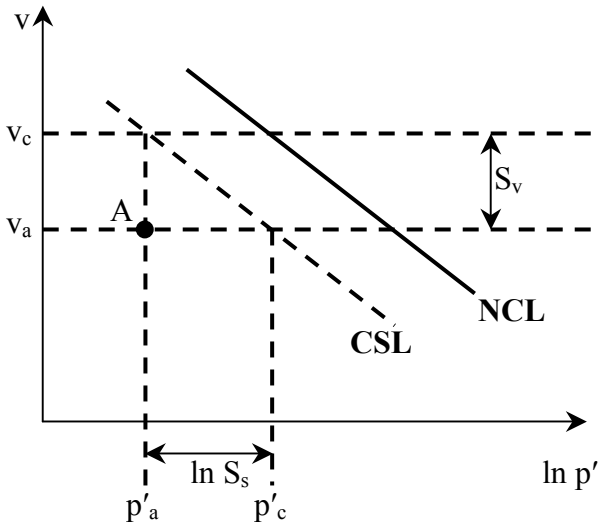

Fig. 3.4: State parameters.

The gradient λ of the critical state line in the v:ln p′ space is generally less than unity for most soils. Therefore, a large variation in p′ would result in only a small change in void ratio. This is especially true for sands where the critical state line is much flatter than clays. A volumetric based state parameter S_v may not capture such large variations in stress. Therefore, the stress based state parameter S_p may be a better measure for characterizing the state of sand (Pillai and Muhunthan, 2003; Klotz and Coop, 2001).

3.3 Family of critical state lines

Schofield and Wroth (1968) have summarized the results of critical state lines of different clays obtained by researchers as shown in Fig. 3.5. It can be seen that the geometrical extension of these lines leads to an interesting behavior; all lines pass through or very near, a single point Ω given by $\upsilon_\Omega \approx 1.25$, $p_\Omega \approx 10300$ kPa.

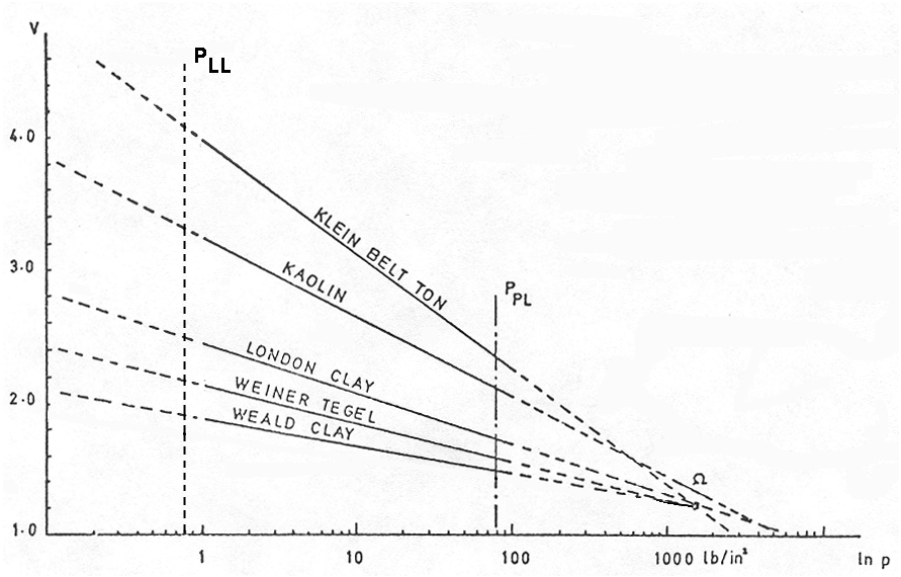

Fig. 3.5: Family of experimental critical state lines.

Lawrence (1980) carried out a series of experiments on different mixtures of Kaolin clay and established the critical state line in a diagram similar to that used by Schofield and Wroth (1968) as shown in Fig. 3.6. It can be seen that for these mixtures the Ω point is slightly different with $\upsilon_\Omega \approx 1.33$ and $p_\Omega \approx 10300$ kN/m^2.

An idealized plot of a family of critical state lines through Ω with υ=1.25 and p'=10300 kN/m^2 is shown in Fig. 3.7. Note that this extrapolation is clearly unlikely to be justified experimentally because besides any question of fracture and degradation of the soil particles under such high pressures, the lines cannot cross and must be asymptotic to

the line υ=1 which represents a specimen with zero voids (Schofield and Wroth, 1968). However, this idealization is useful to characterize the critical state line of a number of clays as a family of lines with a common initiation point Ω (Schofield and Wroth, 1968).

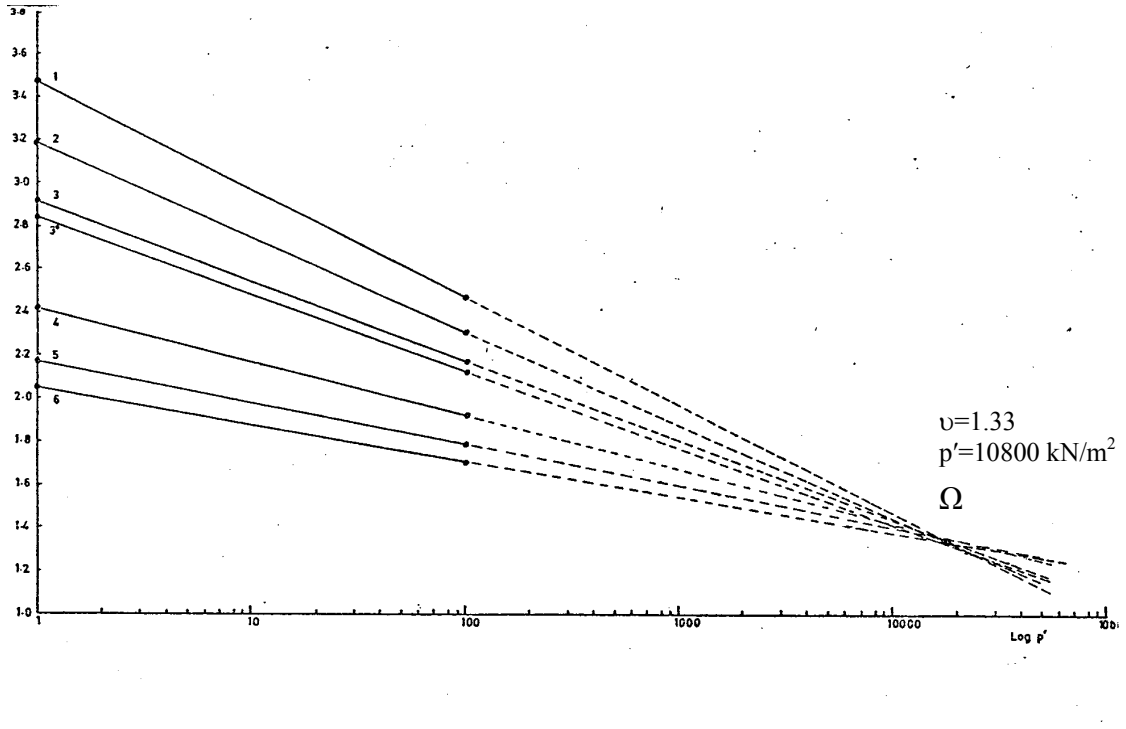

Fig. 3.6: Critical state lines for Kaolin mixtures (Lawrence, 1980).

3.4 Material properties of the mix soil

The plan and cross-sectional view of the sand columns with diameter D installed in a soil with spacing S are as shown in Fig. 3.8. Consider a square unit cell with spacing S within the improved area with a sand column at its center. For analysis purposes, the unit cell can be approximated to be an equivalent circular area. The volume fraction of the in situ soil and the sand column material can be assumed to be equal to the area fraction.

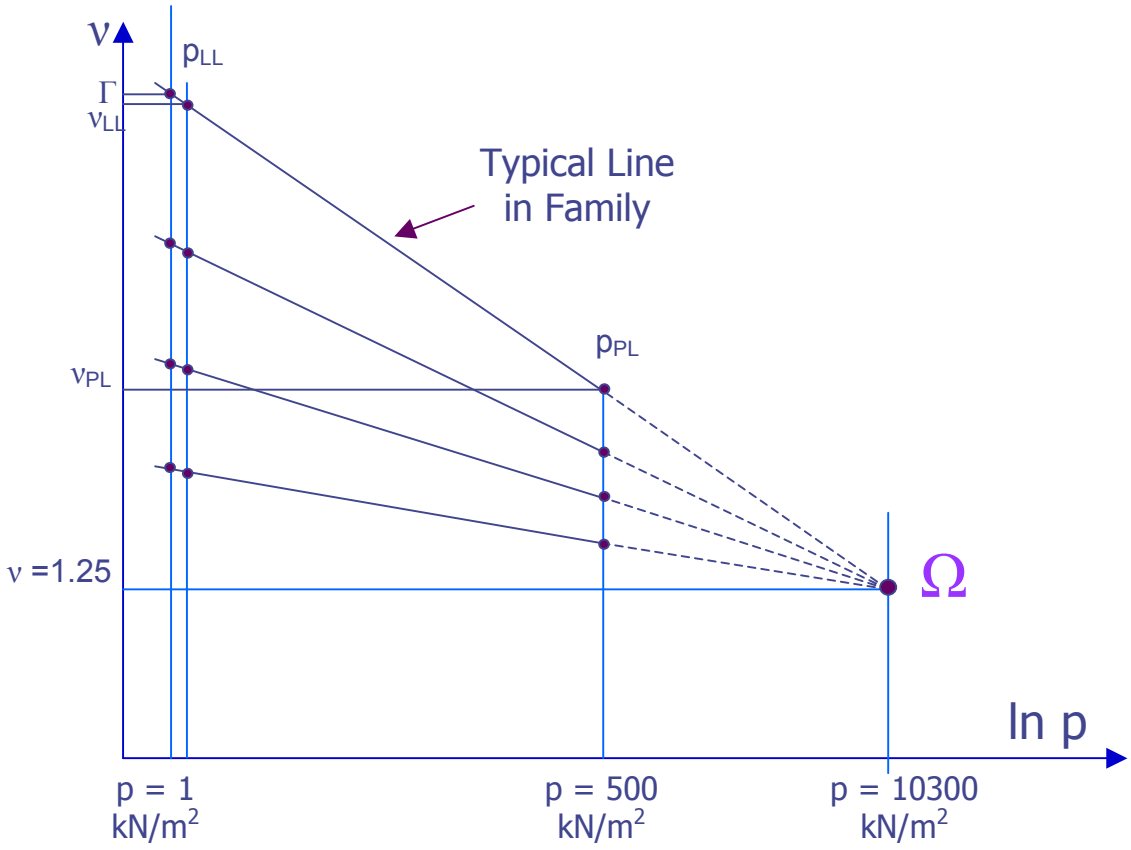

Fig. 3.7: Idealized family of critical state lines.

The ratio between the area of sand column and the total area of a unit cell is defined as the improved area ratio a, then

$$a = \frac{A_c}{A_T} \tag{3-14}$$

where A_c is the horizontal area of a column material and A_T is the horizontal area of the unit cell. Note that a is similar to the replacement ratio as used by Bergado et al., (1996).

The ratio between the total volume of the column material to the total volume of the in situ clay, can be defined as the volume ratio V.R:

$$V.R = \frac{V_c}{V_s} \tag{3-15}$$

where V_c, V_s are the volumes of column material and the in-situ soil. For sand columns placed through the full depth of the clay layer, V.R will equal the ratio between the horizontal areas of the columns to the horizontal area of the in-situ clayey soil. Hence,

$$V.R = \frac{V_c}{V_s} = \frac{A_c}{A_T - A_c} \tag{3-16}$$

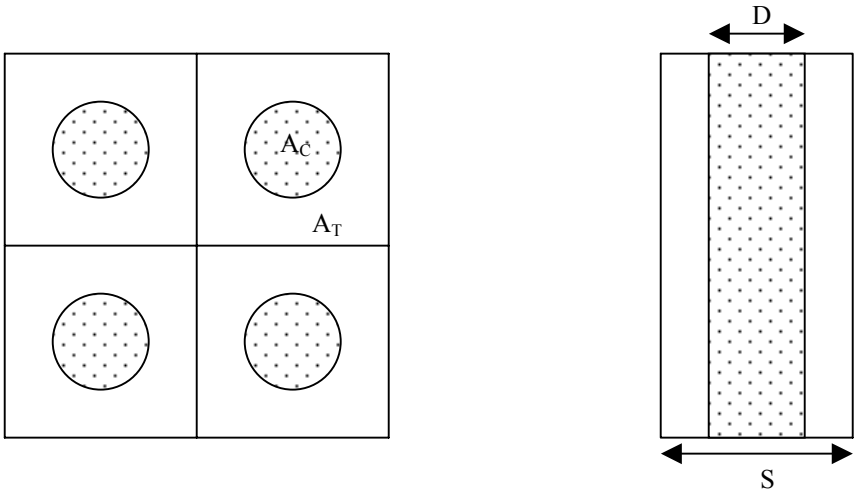

Fig. 3.8: Schematic diagram of the sand columns

Eq. 3-16 can be rewritten as:

$$V.R = \frac{A_c / A_T}{1 - A_c / A_T} \tag{3-17}$$

Substituting Eq. 3-14 into Eq. 3-17 leads to:

$$V.R = \frac{a}{1 - a} \tag{3-18}$$

Let the specific volumes of the column material and the in situ soil be υ_c and υ_s respectively. Accordingly,

$$\upsilon_c = \frac{\text{Total Volume of Column Material, } V_c}{\text{Volume of Solids in Column material, } V_{sc}} \tag{3-19}$$

$$\upsilon_s = \frac{\text{Total Volume of Weak Soil, } V_s}{\text{Volume of Solids in Weak Soil, } V_{ss}} \tag{3-20}$$

Then the specific volume of the composite (mix soil) will be:

$$\upsilon = \frac{\text{Total Volume of Composite, } V}{\text{Volume of Solids in Composite, } V_s}$$

ie:,

$$\upsilon = \frac{V}{V_s} = \frac{V_c + V_s}{V_{sc} + V_{ss}} \tag{3-21}$$

Note that the above summation of individual components assumes that the materials remain intact and that no mixing of sand and in-situ soil takes place. This assumption may not hold for the small interface region between the sand column and in-situ soil.

Eq. 3-21 can be re written as:

$$\upsilon = \frac{V_c/V_s + 1}{V_{sc}/V_s + V_{ss}/V_s} = \frac{V_c/V_s + 1}{V_{sc}/V_c \times V_c/V_s + V_{ss}/V_s} \tag{3-22}$$

Substitution of Eq. 3-10 into Eq. 3-22 results in:

$$\upsilon = \frac{V.R + 1}{V.R/\upsilon_c + 1/\upsilon_s} \tag{3-23}$$

Eq. 3-23 can be rewritten as:

$$\upsilon = \frac{(V.R + 1)\upsilon_c\upsilon_s}{V.R \times \upsilon_s + \upsilon_c} \tag{3-24}$$

Using Eqs. 3-24 and 3-23 the specific volume of the composite can be written as a function of the improved area ratio a as:

$$\upsilon = \frac{(\frac{a}{1-a}+1)\upsilon_c\upsilon_s}{\frac{a}{1-a}\times\upsilon_s+\upsilon_c} \tag{3-25}$$

Eq. 3-25 can be simplified to:

$$\upsilon = \frac{\upsilon_c\upsilon_s}{a\upsilon_s+(1-a)\upsilon_c} \tag{3-26}$$

The above relationship is useful to find the specific volume of the mix as a function of the improved area ratio a, υ_s and υ_c. Since the family of critical state lines for the mix of soils pass through the Ω point (υ=1.25 and p′=10300 kN/m^2) in the υ: ln p′ space, the slope λ of a line corresponding to given mix can be calculated using its specific volume at 1 kPa calculated by means of Eq. 3-26. The slope of the elastic line κ is then assumed to be a function of λ. Eq. 3-26 is also useful to calculate the initial void ratio changes of the mixture. Furthermore, the elastic young modulus of the improved ground is assumed to vary as a function of the area ratio.

CHAPTER 4

CONSTITUTIVE MODELS IN FLAC 3D

4.1 FLAC 3D

FLAC 3D (Fast Lagrangian Analysis of Continua in 3D) is an advanced tool for studying complex interaction of ground-rock/structures in geotechnical engineering. It is a three-dimensional explicit finite-difference program developed by Itasca Consulting Group, Inc, USA (FLAC 3D, 2002). It can be used to solve problems involving mechanical loading capacity and deformations, evaluation of progressive failure and collapse, factor-of-safety calculation, fully and partially saturated fluid flow, pore pressure build-up and dissipation for undrained and drained loading, and dynamic analysis.

FLAC 3D contains a powerful built-in programming language, FISH, that enables the user to define new variables and functions. FISH offers a unique capability to users who wish to tailor the analysis to suit their specific needs.

The formulation of FLAC 3D is adapted perfectly to the modeling of the problems of geomechanics in several phases, like a sequence excavation - construction - loading.

Several types of fluid/solid interaction can be specified in FLAC 3D. It can calculate pore-pressure effects with or without pore-pressure dissipation. This is useful to simulate drained and undrained analyse.

FLAC 3D offers a large number of constitutive models. This study uses the Modified cam clay model (Roscoe and Burland, 1968) and the Mohr- Coulomb model. The brief description of the models is provided here for completeness. For a detailed description the reader is reffered to the FLAC 3D Manual (2002).

4.2 Modified Cam-Clay model

The theory used for this model based on the critical state plasticity theory and the modified Cam-Clay theory developed by Roscoe and Burland (1968) and Wood (1990). The modified Cam-Clay model is an incremental hardening/softening elasto plastic model. Its features include a particular form of nonlinear elasticity and hardening/softening behavior governed by volumetric plastic strain ("density" driven). The failure envelopes are self-similar in shape and correspond to ellipsoids of rotation about the mean stress axis in the principal stress space. The shear flow rule is associated; no resistance to tensile mean stress is offered in this model.

4.2.1 Incremental elastic law

The generalized stress components involved in the model definition are the mean effective pressure, p and deviatoric stress, q, defined as:

$$\begin{aligned} p &= -\frac{1}{3}\sigma_{ii} \\ q &= \sqrt{3J_2} \end{aligned} \tag{4-1}$$

Where the Einstein summation convention applies and J_2 is the second invariant of the effective deviatoric-stress tensor:

$$J_2 = \frac{1}{2}s_{ij}s_{ij} \tag{4-2}$$

The incremental strain variables associated with p and q are the volumetric strain increment $\Delta\varepsilon_p$ and shear strain increment $\Delta\varepsilon_q$, and we have:

$$\begin{aligned} \Delta\varepsilon_p &= -\Delta\varepsilon_{ii} \\ \Delta\varepsilon_q &= \frac{2}{3}\sqrt{3\Delta J'_2} \end{aligned} \tag{4-3}$$

where $\Delta \mathbf{J}'_2$ is the second invariant of the incremental deviatoric-strain tensor:

$$\Delta J'_2 = \frac{1}{2}\Delta e_{ij}\Delta e_{ij} \tag{4-4}$$

In the FLAC 3D plastic flow formulation, both plastic and elastic principal strain-increment vectors are assumed coaxial with the current principal stress vector. The generalized strain increments are then decomposed into elastic and plastic parts so that:

$$\begin{aligned} \Delta\varepsilon_p &= \Delta\varepsilon_p^e + \Delta\varepsilon_p^p \\ \Delta\varepsilon_q &= \Delta\varepsilon_q^e + \Delta\varepsilon_q^p \end{aligned} \tag{4-5}$$

The evolution parameter is the specific volume, υ, defined as:

$$\upsilon = \frac{V}{V_s} \tag{4-6}$$

where V_s is the volume of solid particles, assumed incompressible, contained in a volume, V ,of soil. The incremental relation between volumetric strain, ε_p , and specific volume has the form:

$$\Delta\varepsilon_p = -\frac{\Delta\upsilon}{\upsilon} \tag{4-7}$$

and the new specific volume, υ^N , for the step may be calculated as:

$$\upsilon^N = \upsilon\left(1 - \Delta\varepsilon_p\right) \tag{4-8}$$

The incremental expression of Hooke's law in terms of generalized stress and strains is as follows:

$$\begin{aligned} \Delta p &= K\Delta\varepsilon_p^e \\ \Delta q &= 3G\Delta\varepsilon_q^e \end{aligned} \tag{4-9}$$

where

$$\Delta J_2 = \frac{1}{2}\Delta s_{ij}\Delta s_{ij} \qquad (4\text{-}10)$$

In the Modified cam-clay model, the tangential bulk modulus, K, in the volumetric relation Eq. 4-9 is updated to reflect a nonlinear law derived experimentally from isotropic compression tests. The results of a typical isotropic compression test are presented in the semi-logarithmic plot of Fig. 4.1 .

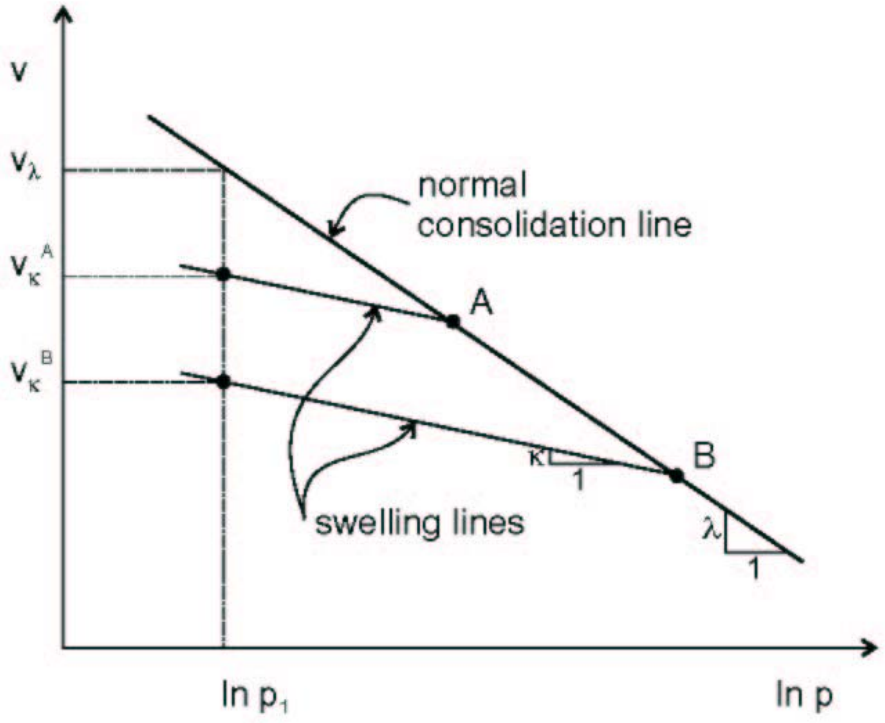

Fig. 4.1: Normal consolidation line and unloading-reloading (swelling) line for an isotropic compression test (FLAC 3D, 2002)

As the normal consolidation pressure, p , increases, the specific volume, υ, of the material decreases. The point representing the state of the material moves along the normal consolidation line defined by:

$$\upsilon = \upsilon_{\lambda} - \lambda \ln \frac{p}{p_1} \tag{4-11}$$

where λ and υ_{λ} are two material parameters and p_1 is a reference pressure. (Note that υ_{λ} is the value of the specific volume at the reference pressure.)

An unloading-reloading excursion, from point A or B on the figure, will move the point along an elastic swelling line of slope κ , back to the normal consolidation line where the path will resume. The equation of the swelling lines has the form:

$$\upsilon = \upsilon_{\kappa} - \kappa \ln \frac{p}{p_1} \tag{4-12}$$

where κ is a material constant, and the value of υ_{κ} for a particular line depends on the location of the point on the normal consolidation line from which unloading was performed - i.e., υ_{κ}^{A} for unloading from point A , and υ_{κ}^{B} for unloading from point B in Fig. 4.1 .

The recoverable change in specific volume, $\Delta\upsilon^{e}$, may be expressed in incremental form after differentiation of Eq. 4-12:

$$\Delta\upsilon^{e} = -\kappa \frac{\Delta p}{p} \tag{4-13}$$

After division of both members by υ, and using Eq. 4-7, we may write:

$$\Delta p = \frac{\upsilon p}{\kappa} \Delta\varepsilon_{p}^{e} \tag{4-14}$$

In the modified cam-clay model it is assumed that any change in mean pressure is accompanied by elastic change in volume according to the above expression. Comparison with Eq. 4-9 hence suggests the following expression for the tangent bulk modulus of the modified cam-clay material:

$$K = \frac{\upsilon p}{\kappa} \tag{4-15}$$

Under more-general loading conditions, the state of a particular point in the medium might be represented by a point, such as A , located below the normal consolidation line in the (υ, ln p) plane (see Fig. 4.2). By virtue of the law adopted in Eq. 4-12 , an elastic path from that point proceeds along the swelling line through A .

The specific volume, υ_C^A and mean pressure, p_C^A at the intersection of swelling line and normal consolidation line are referred to as (normal) consolidation (specific) volume and (normal) consolidation pressure respectively. Consider an incremental change in stress bringing the point from state A to state A′. At A′ there corresponds a consolidation volume, $\upsilon_c^{A'}$, and consolidation pressure, $p_c^{A'}$. The increment of plastic volume change, $\Delta\upsilon p$, is measured on the figure by the vertical distance between swelling lines (associated with points A and A′) and we may write, using incremental notation:

$$\Delta\upsilon^p = -(\lambda - \kappa)\frac{\Delta p_c}{p_c} \tag{4-16}$$

After division of the left and right member by υ , we obtain, comparing with Eq. 4-7:

$$\Delta\varepsilon_p^p = \frac{\lambda - \kappa}{\upsilon}\frac{\Delta p_c}{p_c} \tag{4-17}$$

Hence, whereas elastic volume changes take place whenever the mean pressure changes, plastic volume changes occur only when the consolidation pressure changes.

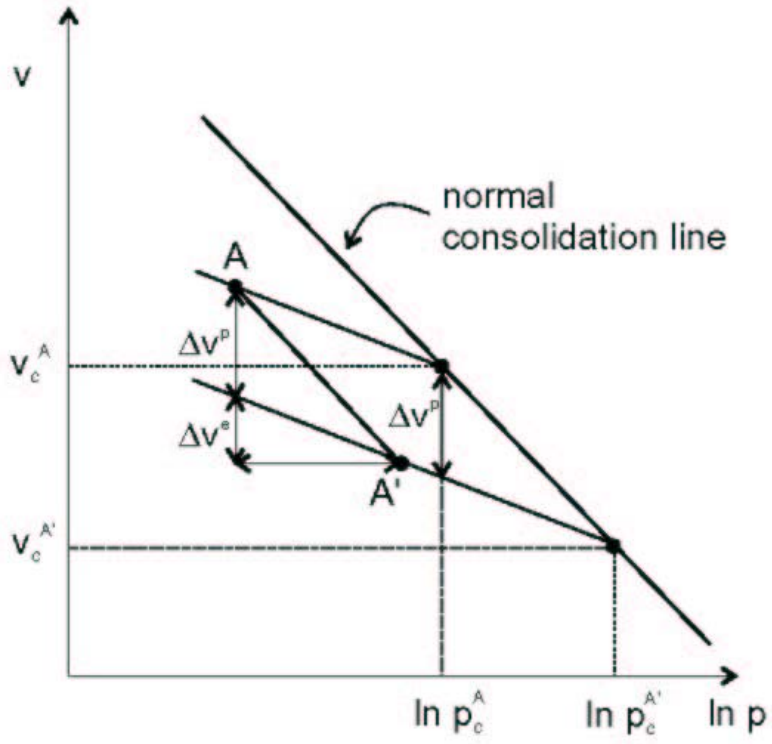

Fig. 4.2: Plastic volume change corresponding to an incremental consolidation pressure change (FLAC 3D, 2002)

4.2.2 Yield and potential functions

The yield function corresponding to a particular value p_c of the consolidation pressure has the form:

$$f(q,p) = q^2 + M^2 p(p - p_c) \tag{4-18}$$

where M is a material constant. The yield condition f = 0 is represented by an ellipse with horizontal axis, p_c , and vertical axis, Mp_c , in the (q,p) -plane (see Fig. 4.3). Note that the ellipse passes through the origin; hence, the material in this model is not able to support an all-around tensile stress.

The failure criterion is represented in the principal stress space by an ellipsoid of

rotation about the mean stress axis (any section through the yield surface at constant mean effective stress, p ,is a circle).

The potential function, g , corresponds to an associated flow rule and we have:

$$g = q^2 + M^2 p\left(p - p_c\right) \tag{4-19}$$

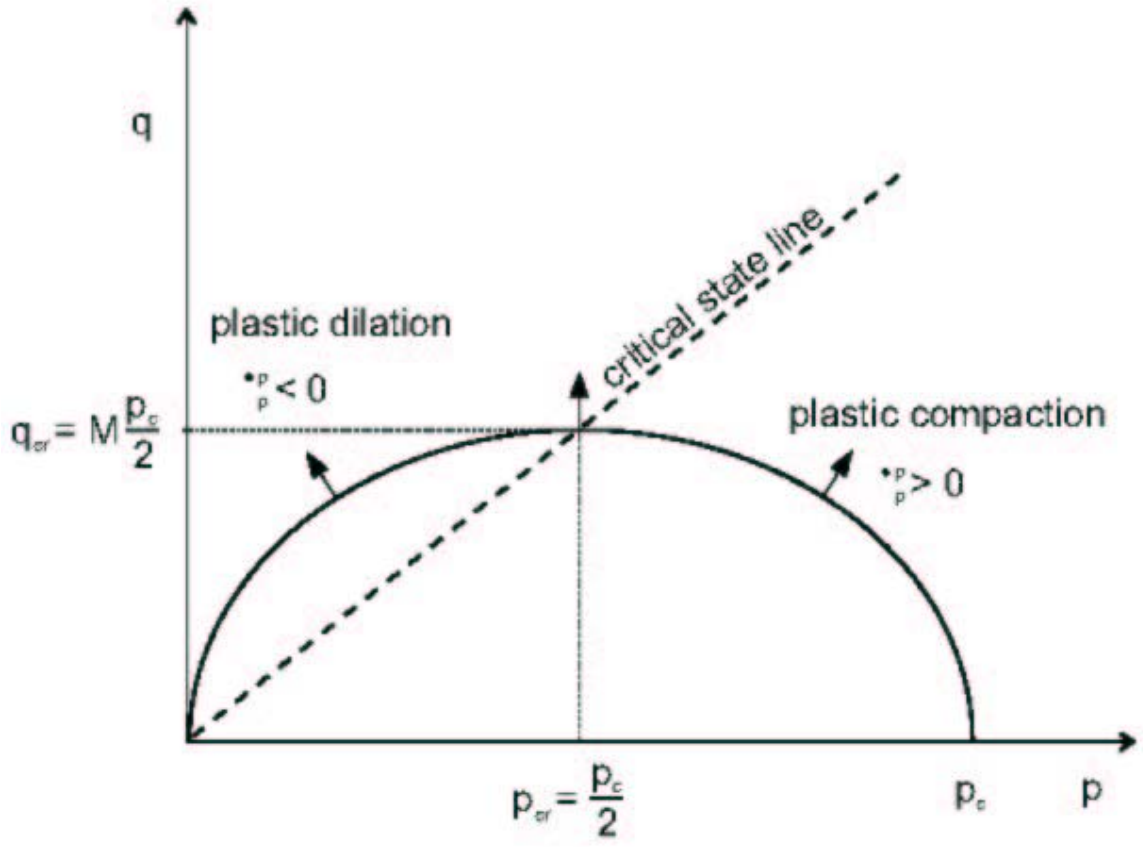

Fig. 4.3: Cam-clay failure criterion in FLAC 3D

4.2.3 Plastic corrections

The flow rule used to describe plastic flow has the form:

$$\Delta\varepsilon_p^p = \lambda^{\upsilon}\frac{\partial g}{\partial P}$$
$$\Delta\varepsilon_q^p = \lambda^{\upsilon}\frac{\partial g}{\partial q} \tag{4-20}$$

where λ^{υ} is the plastic (volumetric) multiplier whose magnitude remains to be defined. Using Eq. 4-19 for g , these expressions give , after partial differentiation:

$$\begin{aligned} \Delta\varepsilon_p^p &= \lambda^{\upsilon} c_a \\ \Delta\varepsilon_q^p &= \lambda^{\upsilon} c_b \end{aligned} \tag{4-21}$$

where

$$\begin{aligned} c_a &= M^2\left(2p - p_c\right) \\ c_b &= 2q \end{aligned} \tag{4-22}$$

The elastic strain increments may be expressed from Eq. 4-5 as total minus plastic increments. In further using Eq. 4-21 , the elastic laws in Eq. 4-9 become:

$$\begin{aligned} \Delta p &= K(\Delta(_p - \lambda^{\upsilon} c_a) \\ \Delta q &= 3G(\Delta(_q - \lambda^{\upsilon} c_b) \end{aligned} \tag{4-23}$$

Let the new and old stress states be referred to by the superscripts N and O , respectively . Then, by definition, for one step:

$$\begin{aligned} p^N &= p^O + \Delta p \\ q^N &= q^O + \Delta q \end{aligned} \tag{4-24}$$

Substitution of Eq. 4-23 gives:

$$\begin{aligned} p^N &= p^I - \lambda^{\upsilon} K c_a \\ q^N &= q^I - \lambda^{\upsilon} 3G c_b \end{aligned} \tag{4-25}$$

where the superscript I is used to represent the elastic guess obtained by adding to the old stresses, elastic increments are computed using the total strain increments - i.e.,

$$p^I = p^O + K\Delta\varepsilon_p$$
$$q^I = q^O + 3G\Delta\varepsilon_q \tag{4-26}$$

The parameter λ^v may now be defined by requiring that the new stress point be located on the yield surface. Substitution of p^N and q^N, as given by Eq. 4-25, for p and q in f(q,p) = 0, gives, after some manipulations (see Eq. 4-18)):

$$a\left(\lambda^v\right)^2 + b\lambda^v + c = 0 \tag{4-27}$$

where

$$a = \left(MKc_a\right)^2 + \left(3Gc_b\right)^2$$
$$b = -\left[Kc_a c_a^I + 3Gc_b c_b^I\right] \tag{4-28}$$
$$c = f\left(q^I, p^I\right)$$

Of the two roots of this equation, the one with the smallest magnitude must be retained. Note that at the critical point corresponding to $p_{cr} = p_c/2$, $q_{cr} = M p_c/2$ in Fig. 4.3, the normal to the yield curve f = 0 is parallel to the q -axis. Since the flow rule is associated, the plastic volumetric strain-rate component vanishes there. As a result of the hardening rule Eq. 4-17, the consolidation pressure, p_c, will not change. The corresponding material point has reached the critical state in which unlimited shear strains occur with no accompanying change in specific volume or stress level.

The new stress components, σ_{ij}^N, are expressed in terms of old and new generalized stress values, using the expressions:

$$\sigma_{ij}^N = s_{ij}^N + p^N\delta_{ij} \tag{4-29}$$

where

$$s_{ij}^N = s_{ij}^I \frac{q^N}{q^I} \tag{4-30}$$

and [s] is the deviatoric stress tensor.

4.2.4 Hardening/Softening rule

The size of the yield curve is dependent on the value of the consolidation pressure, p_c (Eq. 4-18). This pressure is a function of the plastic volume change and varies with the specific volume as indicated in Eq. 4-17. The consolidation pressure is updated for the step, using the formula:

$$p_c^N = p_c\left(1 + \Delta\varepsilon_p^p \frac{\upsilon}{\lambda - \kappa}\right) \tag{4-31}$$

where $\Delta\varepsilon_p^p$ is the plastic volumetric strain increment for the step, υ is the current specific volume and λ and κ are material parameters, as given previously in Eq. 4-11.

4.2.5 Initial stress state

The Modified cam-clay model in FLAC 3D is only applicable to a material in which the stress state corresponds to a compressive mean effective stress. This model is not designed to predict the behavior of material in which this condition is not met. In particular , the initial state of the material (just before application of the Cam-clay model) must be consistent with this requirement. The initial stress state may be specified using the INITIAL command or may be the result of a run in which another constitutive model has been used. An error message will be issued if the Cam-clay model is applied to a zone where the initial effective pressure, defined as p_0 ,is negative .

4.2.6 Over consolidation ratio

The over-consolidation ratio, R, is defined as the ratio between the zone initial preconsolidation pressure (a material property) and initial pressure, p_0 - i.e.:

$$R = \frac{p_{c0}}{p_0} \tag{4-32}$$

This ratio is useful in characterizing the behavior of Cam-clay material.

4.2.7 Implementation procedure

In the implementation of the Cam-clay model in FLAC 3D , an elastic guess, σ_{ij}^{I} , is first computed after adding to the old stress components, increments calculated by application of Hooke's law to the total strain increment for the step.

Elastic guesses for the mean pressure, p^I , and deviatoric stress, q^I , are calculated using Eq. 4-1. If these stresses violate the criterion for yield and $f(q^I, p^I) > 0$ (see Eq. 4-18), plastic deformation takes place and the consolidation pressure must be updated. In this situation, a correction must be applied to the elastic guess to give the new stress state. New stresses p^N and q^N are first evaluated from Eq. 4-25 using the expression for λ corresponding to the root of Eqs. 4-27 and 4-28 with smallest magnitude. Note that, in this version of the code, the expressions in Eq. 4-22 for c_a and c_b are evaluated using the elastic guess; the error associated with this technique is expected to be small, provided the steps are small. New stress tensor components in the system of reference axes are hence evaluated using Eqs. 4-29 and 4-30.

Volumetric strain increment, $\Delta\varepsilon_p$, and mean pressure, p , for the zone are

computed as an average over all involved tetrahedra - see Eqs. 4-1 and 4-3. The zone volumetric strain, ε_p , is incremented and the zone specific volume, υ , updated using Eq. 4-8. In turn, the new zone consolidation pressure is calculated from Eq. 4-31 , and the tangential bulk modulus is updated using formula Eq. 4-15.

If a nonzero value for the Poisson ratio property is imposed, a new shear modulus is calculated from the expression $G = \frac{1.5(1-2\nu)K}{(1+\nu)}$. Otherwise, G is left unchanged as long as the condition $0 \le \nu \le 0.5$ is satisfied; if it is not, G is assigned a value for υ=0 or υ = 0.5, as appropriate.

The new values for the consolidation pressure, and shear and bulk moduli are then stored for use in the next time step. The material properties thus lag one time step behind the corresponding calculation. In an explicit code, this error is small because the steps are small.

4.3 Mohr-Coulomb model

The failure envelope for this model corresponds to a Mohr -Coulomb criterion (shear yield function) with tension cutoff (tension yield function) (Fig. 4.4). The position of a stress point on this envelope is controlled by a non-associated flow rule for shear failure and an associated rule for tension failure.

4.3.1 Generalized stress and strain components

The Mohr -Coulomb criterion in FLAC 3D is expressed in terms of the principal stresses σ_1, σ_2 and σ_3, which are the three components of the generalized stress vector for this model (n = 3). The components of the corresponding generalized strain vector are the

principal strains ε_1, ε_2 and ε_3.

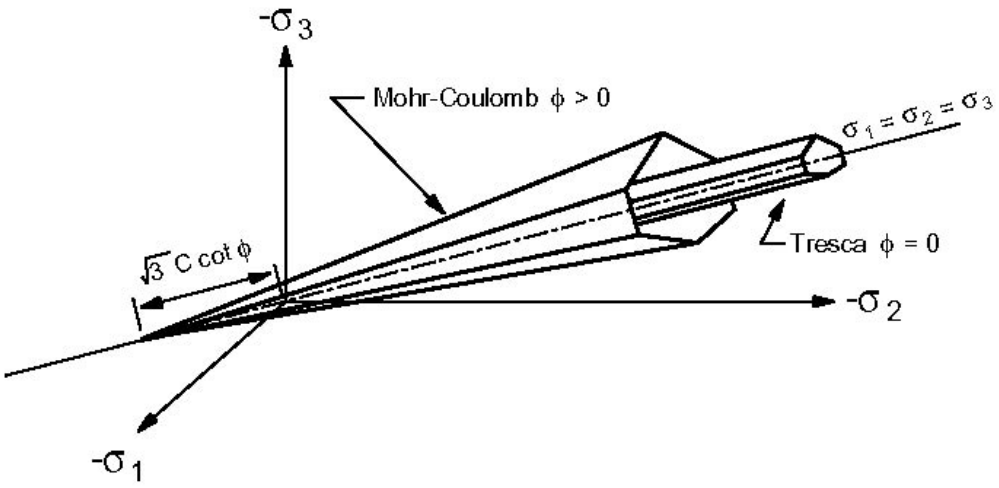

Fig. 4.4: Mohr-Coulomb and Tresca yield surfaces in principal stress space (FLAC 3D, 2002)

4.3.2 Incremental elastic law

The incremental expression of Hooke's law in terms of the generalized stress and stress increments has the form

$$\Delta\sigma_1 = \alpha_1 \Delta\varepsilon_1^e + \alpha_2 \left(\Delta\varepsilon_2^e + \Delta\varepsilon_3^e\right)$$

$$\Delta\sigma_2 = \alpha_1 \Delta\varepsilon_2^e + \alpha_2 \left(\Delta\varepsilon_1^e + \Delta\varepsilon_3^e\right) \qquad (4\text{-}33)$$

$$\Delta\sigma_3 = \alpha_1 \Delta\varepsilon_3^e + \alpha_2 \left(\Delta\varepsilon_1^e + \Delta\varepsilon_2^e\right)$$

where α_1 and α_2 are material constants defined in terms of the shear modulus, G , and bulk modulus, K , as:

$$\alpha_1 = K + \frac{4}{3}G$$

$$\alpha_2 = K - \frac{2}{3}G \tag{4-34}$$

For future reference, comparing those expressions with the elastic relations between elastic strain increments and stress increments ($\Delta\underline{\sigma}_i = S_i\left(\Delta\underline{\varepsilon}_n^e\right)$ $i = 1, n$ where S_i is a linear function of the elastic strain increments $\Delta\underline{\varepsilon}_n^e$), we may write:

$$\begin{aligned} S_1\left(\Delta\varepsilon_1^e, \Delta\varepsilon_2^e, \Delta\varepsilon_3^e\right) &= \alpha_1\Delta\varepsilon_1^e + \alpha_2\left(\Delta\varepsilon_2^e + \Delta\varepsilon_3^e\right) \\ S_2\left(\Delta\varepsilon_1^e, \Delta\varepsilon_2^e, \Delta\varepsilon_3^e\right) &= \alpha_1\Delta\varepsilon_2^e + \alpha_2\left(\Delta\varepsilon_1^e + \Delta\varepsilon_3^e\right) \\ S_3\left(\Delta\varepsilon_1^e, \Delta\varepsilon_2^e, \Delta\varepsilon_3^e\right) &= \alpha_1\Delta\varepsilon_3^e + \alpha_2\left(\Delta\varepsilon_1^e + \Delta\varepsilon_2^e\right) \end{aligned} \tag{4-35}$$

4.3.3 Composite failure criterion and flow rule

The failure criterion used in the FLAC 3D model is a composite Mohr -Coulomb criterion with tension cutoff. In labeling the three principal stresses so that:

$$\sigma_1 \le \sigma_2 \le \sigma_3 \tag{4-36}$$

this criterion may be represented in the plane (σ_1, σ_3) as illustrated in Fig. 4.5. (compressive stresses are negative).

The failure envelope $f(\sigma_1, \sigma_3) = 0$ is defined from point A to B by the Mohr - Coulomb failure criterion $f^s = 0$ with:

$$f^s = \sigma_1 - \sigma_3 N_\phi + 2c\sqrt{N_\phi} \tag{4-37}$$

and from B to C by a tension failure criterion of the form $f^t = 0$ with:

$$f^t = \sigma_3 - \sigma^t \tag{4-38}$$

where φ is the friction angle, c , the cohesion, σ^t , the tensile strength, and:

$$N_\phi = \frac{1+\sin(\phi)}{1-\sin(\phi)} \tag{4-39}$$

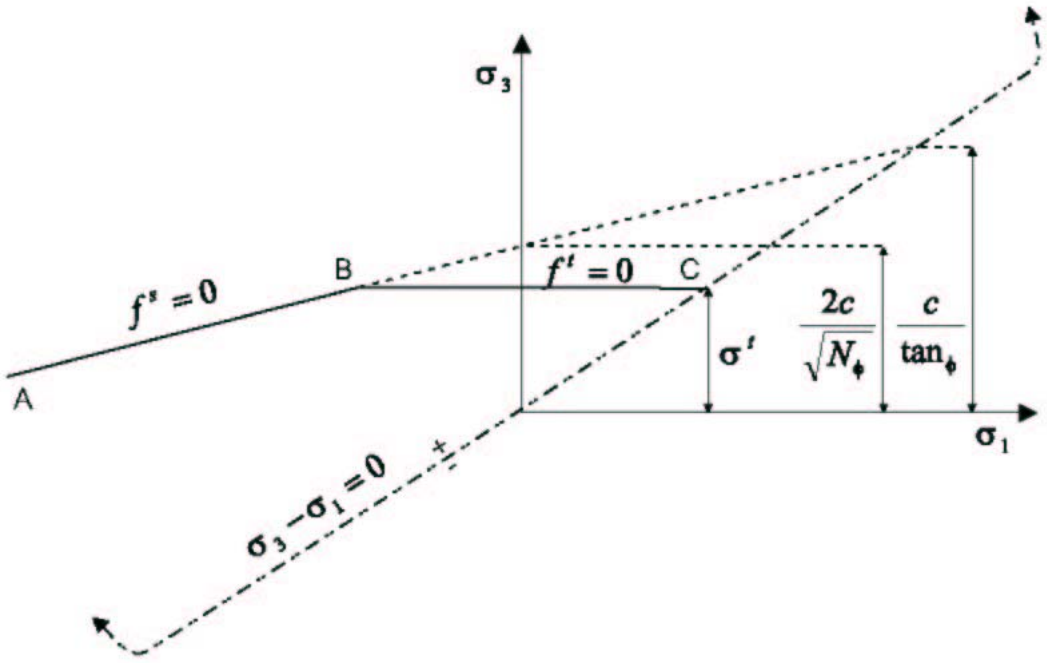

Fig. 4.5: FLAC 3D Mohr-Coulomb failure criterion

Note that the tensile strength of the material cannot exceed the value of σ_3 corresponding to the intersection point of the straight lines $f^s = 0$ and $\sigma_1 = \sigma_3$ in the $f(\sigma_1, \sigma_3)$ plane. This maximum value is given by:

$$\sigma^t_{max} = \frac{c}{\tan\varphi} \tag{4-40}$$

The potential function is described by means of two functions, g^s and g^t , used to define shear plastic flow and tensile plastic flow, respectively. The function g^s

corresponds to a non-associated law and has the form:

$$g^S = \sigma_1 - \sigma_3 N_\psi \tag{4-41}$$

where ψ is the dilation angle and:

$$N_\psi = \frac{1+\sin(\psi)}{1-\sin(\psi)} \tag{4-42}$$

The function g^t corresponds to an associated flow rule and is written:

$$g^t = -\sigma_3 \tag{4-43}$$

The flow rule is given a unique definition by application of the following technique. A function $h(\sigma_1,\sigma 3) = 0$ is defined which is represented by the diagonal between the representation of $f^s = 0$ and $f^t = 0$ in the (σ_1,σ_3)-plane (see Fig. 4.6). The function is selected with its positive and negative domains, as indicated on the figure, and has the form:

$$h = \sigma_3 - \sigma^t + a^P\left(\sigma_1 - \sigma^P\right) \tag{4-44}$$

where a^P and σ^P are constants defined as:

$$\begin{aligned} a^P &= \sqrt{1+N_\phi^2} + N_\phi \\ \sigma^P &= \sigma^t N_\phi - 2c\sqrt{N_\phi} \end{aligned} \tag{4-45}$$

An elastic guess violating the composite yield function is represented by a point in the $(\sigma_1,\sigma 3)$-plane located either in domain 1 or 2 , corresponding to negative or positive domains of $h = 0$, respectively (see Fig. 4.6). If the stress point falls within domain 1, shear failure is declared, and the stress point is placed on the curve $f^s = 0$ using a flow rule derived using the potential function g^s . If the point falls within domain 2, tensile failure takes place, and the new stress point conforms to $f^t = 0$ using a flow rule derived

using g^t.

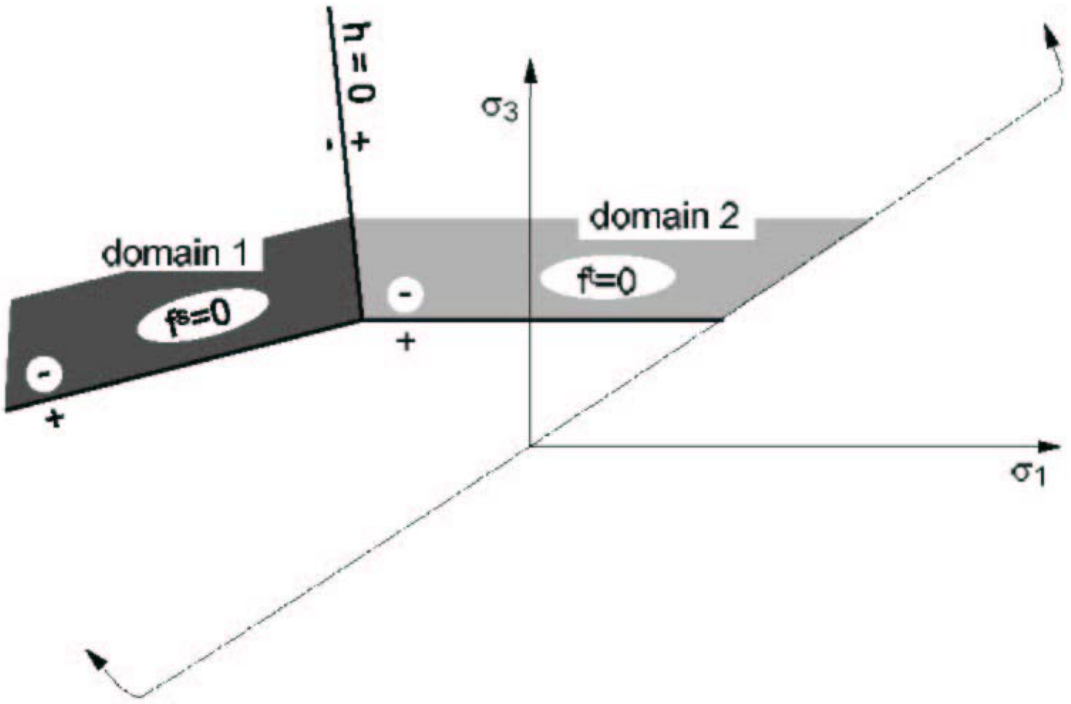

Fig. 4.6: Mohr-Coulomb model – domains used in the definition of the flow rule (FLAC 3D, 2002)

Note that, by ordering the stresses as in Eq. 4-36 , the case of a shear-shear edge is automatically handled by a variation on this technique. The technique, applicable for small-strain increments, is simple to implement: at each step, only one flow rule and corresponding stress correction is involved in case of plastic flow . In particular , when a stress point follows an edge, it receives stress corrections alternating between two criteria. In this process, the two yield criteria are fulfilled to an accuracy which depends on the magnitude of the strain increment. The plastic correction has been performed using the incremental plastic law. (FLAC 3D, 2002)

4.4 Fluid model

A no flow –mechanical generation of pore pressure model is available in FLAC 3D. The undrained (short-term) response may be analyzed in FLAC 3D using both "dry" and "wet" approaches. In a "dry" simulation, the generation of the pore pressure under the volumetric stain is not simulated directly. Instead, its effect on mechanical deformation is taken into account by assigning the undrained bulk value, $K_u = K+\alpha^2M$, to the material bulk modulus, K in the FLAC 3D simulation.

In a "wet" simulation, the short-term response of a coupled system is analyzed in the fluid configuration of FLAC 3D. In this case, drained values should be used for the material bulk modulus, friction and cohesion. The second approach is used in this analysis.

CHAPTER 5

ANALYSIS, RESULTS, AND DISCUSSION

5.1 Verification of FLAC 3D model

The MIT test embankment constructed on Boston Blue clay was one of the most instrumented embankments in the world. The performance of the embankment was carefully monitored by means of hydraulic piezometers, settlement gauges and slope inclinometers. The interpretation of the filed data has been reported in detail by D'Appolonia et al., (1971), Lambe et al., (1972) and Lambe (1973). It has since been used to verify many numerical analyses (Wroth 1979).

A cross section of the embankment is given in Fig. 5.1. The embankment was constructed on an in situ soil consisting mainly of Boston blue clay with a layer thickness of about 18 to 34 m and underlain by a shale layer. A 2 m thick sand layer was located above the Boston blue clay followed by a 2.5 m thick peat layer. Prior to the construction of the embankment, the fill material replaced the peat underneath the embankment region. The filling of the embankment to the surcharge level of elevation +12.2 m (40 ft) was completed by July 1969. A full-scale field trial was conducted in which a length of approximately 100 m (300 ft) of the embankment was filled rapidly until failure occurred.

The field trial provided an opportunity for a special symposium to be held at which the results of genuine Class A predictions (Lambe, 1973) of the performance of the embankment could be compared with the observed behavior (Wroth, 1979).

The available observed field values are as follows:

(1) Additional height of fill necessary to cause a stability failure (differential settlement of the crest of the embankment of 0.15 m (0.5ft) was assumed to constitute a failure).

(2) When 1.8 m (6ft) of fill has been added:

(a) Additional horizontal movement of SI-3 and SI-4 at elevations –11m and –23.1m.

(b) Additional settlement of Settlement plate SP-1

(c) Additional pore-pressures at location P-3, P-4 and P-6

(d) Heave at H-1 and H-2

(3) Additional pore pressures at P-3, P-4 and P-6 at failure.

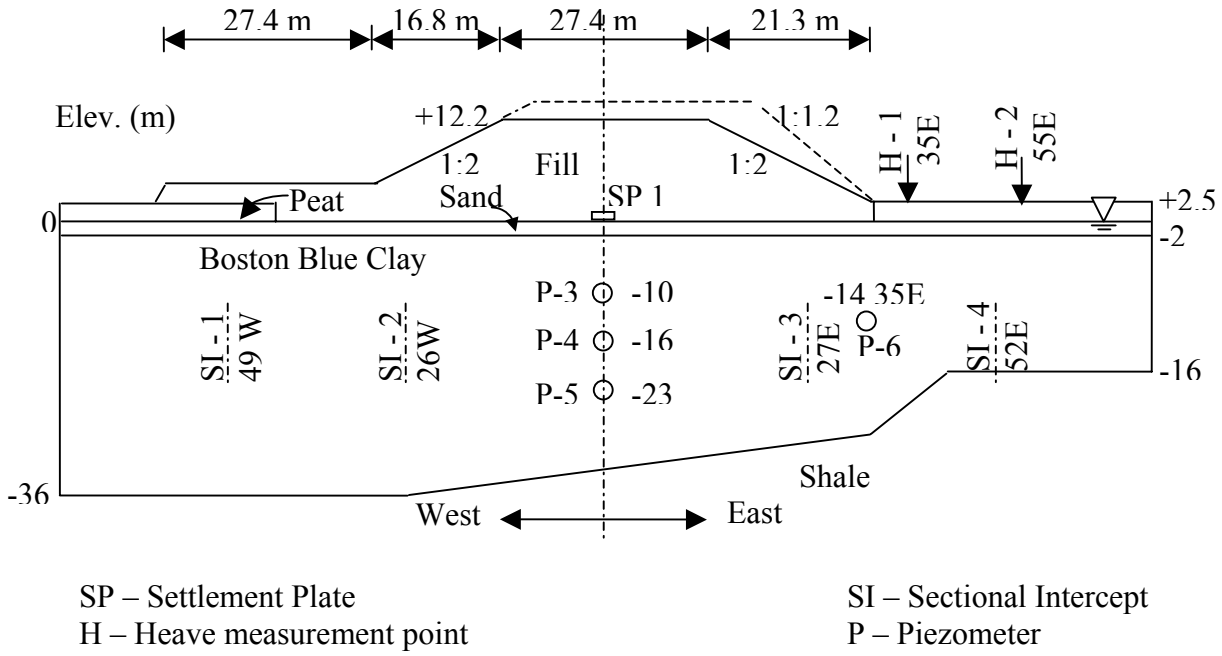

Fig. 5.1: Cross section of the embankment showing ground profile and location of instruments

5.2 Properties of Boston blue clay

The Modified Cam–Clay (MCC) properties of Boston clay were obtained from various research reports (Wroth, 1969, Huang and Chen, 1990, Ladd et al., 1994 and D'Appolonia at el, 1971). The variations of the $C_c/(1+e_0)$ and $C_r/(1+e_0)$ for Boston blue clay are as shown in Fig. 5.2. The variation of the initial void ratio with depth is given in Fig. 5.3.

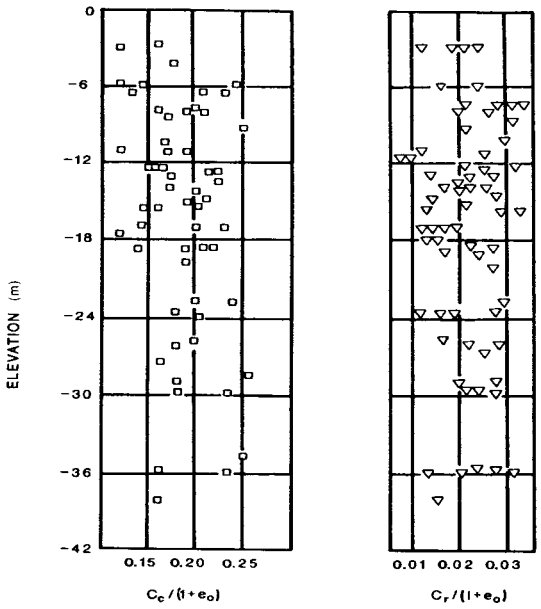

Fig. 5.2: Compression and rebound indexes for Boston blue clay (Huang and Chen, 1990)

Based on the above sets of observations, average values of C_c and C_r were determined to be 0.34 and 0.069, respectively for the present analysis. Accordingly, the slope of the normal compression line λ and slope of elastic swelling line κ become 0.15

and 0.03, respectively, for the MCC model. The friction angle (ϕ') of the Boston Blue Clay is 30^0 which results in the soil constant $M = (6\sin\phi'/(3-\sin\phi')) = 1.2$. The specific volume ($\upsilon_\lambda$) at a reference pressure of 1 MPa is 2.3. Preconsolidation pressure had been taken as mean normal stress multiplied by $\left(1+e_0^2\right)$.

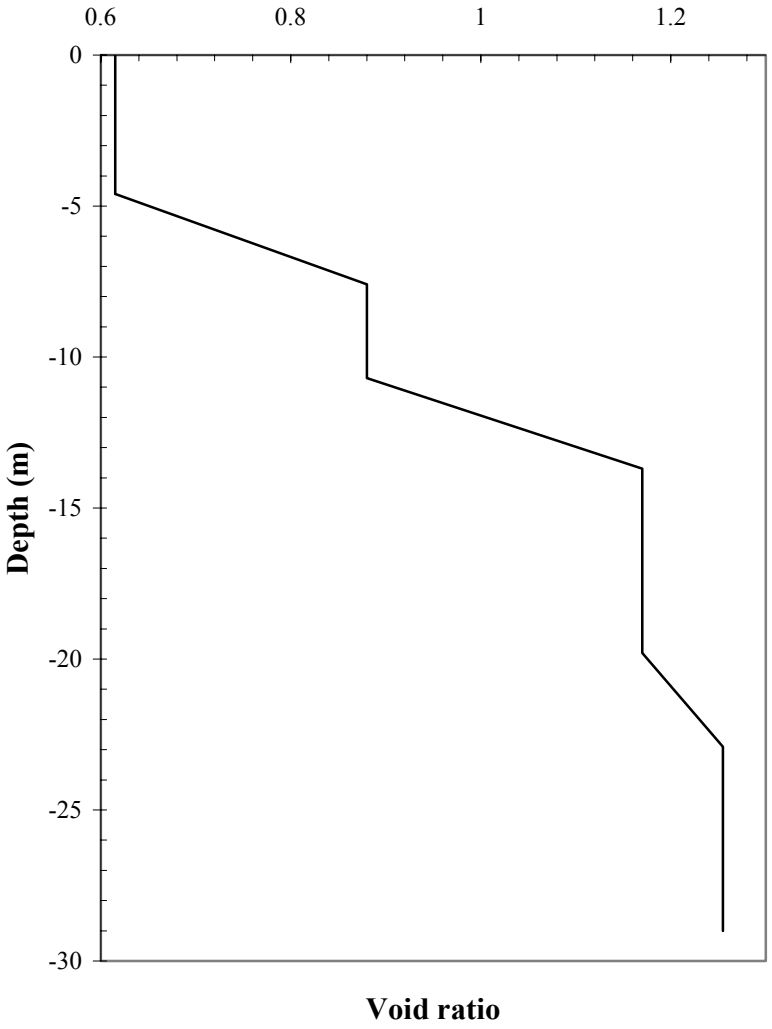

Fig. 5.3: Variation of void ratio with depth for Boston blue clay (Ladd et al., 1994)

Undrained Young's modulus at shallow depths was determined to be 100 MPa from a series of triaxial tests (D'Appolonia at el, 1971). The Poisson's ratio of this clay

was assumed to be 0.35 (Wroth, 1979). Use of these values leads to a shear modulus of 37 Mpa.

The dry density was taken as 1.8 Mg/m^3 and an average porosity of 0.5 was calculated based on the void ratio variation (Fig. 5.3). Accordingly, the saturated density of the clay was calculated to be 2.3 Mg/m^3. Table 5.1 gives a summary of the parameters used for Boston Blue Clay in the numerical analysis

Parameter	Value
Shear Modulus, G (MPa)	37
Soil Constant, M	1.2
Slope of normal consolidation line, λ	0.15
Slope of elastic swelling line, κ	0.03
Reference Pressure, p'_1 (MPa)	1
Specific Volume at reference Pressure, υ_λ	2.3
Dry Density (Mg/m^3)	1.8
Porosity	0.5

Table 5.1: Soil properties of Boston blue clay

5.3 Properties of sand, fill and peat

The sand, fill, and peat were assumed to follow the Mohr- Coulomb constitutive behavior. Strength and deformation parameters are especially difficult to estimate for the fill, marine sand and peat due to the lack of laboratory test data on intact/undisturbed

material. The properties for these materials as shown in Table 5.2 were chosen based on previous research (Ladd at el, 1994).

	Sand	**Fill**	**Peat**
Bulk Modulus, K (MPa)	30	30	0.1
Shear Modulus, G (MPa)	10	10	0.08
Cohesion, c (kPa)	0	4	4
Internal Friction angle, ϕ (Deg)	37	40	25
Dilation angle, ψ (Deg)	0	0	0
Tensile strength, T (kPa)	1	1	1
Dry Density, γ (Mg/m^3)	1.8	1.95	1.2

Table 5.2: Soil Properties for sand, fill, and peat

5.4 FLAC 3D Model of MIT Symposium embankment

FLAC 3D is based upon a command-driven format because most analyses require the use of data input files. In order to set up a model to run a simulation with FLAC 3D, three basic components of a problem need to be specified:

(a) a finite difference grid

(b) constitutive behavior and material properties

(c) boundary and initial conditions

The grid defines the geometry of the problem. Zones are created within a 3D volume by integrating the available basic mesh shapes. The zones and grid arrangements used are shown in Fig. 5.4.

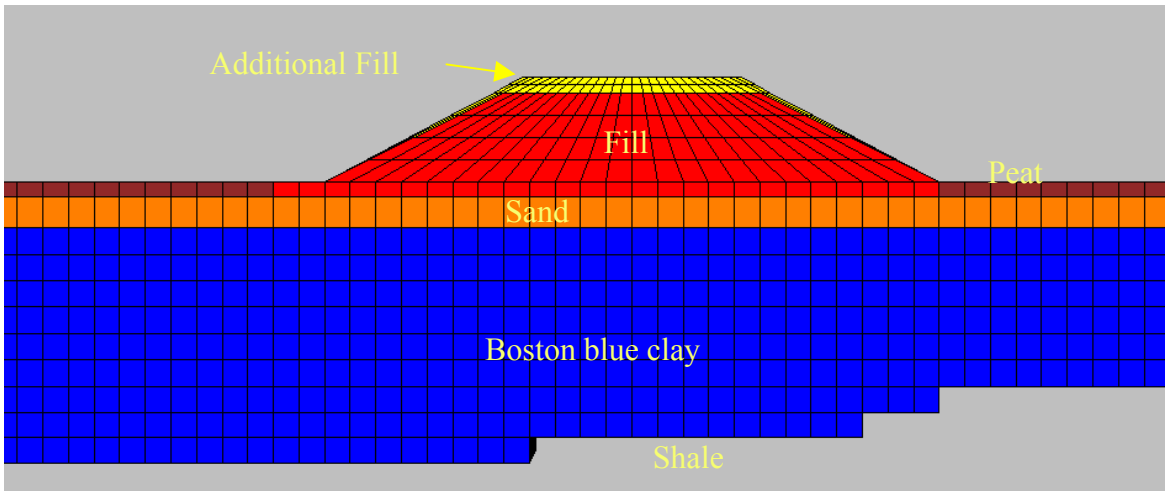

Fig. 5.4: Finite different discretization of the MIT symposium embankment

Modified Cam-Clay model has been used for the constitutive behavior of the Boston Blue Clay with the properties given in Table 5.1. Sand, peat and fill material were assumed to follow the Mohr-Coulomb model with the properties tabulated in Table 5.2 .

Boundary and initial conditions define the in-situ state. For the embankment study here, the x and y displacements along the far ends were restrained. Since the clay layer is underlain by shale all three displacements along the bottom were fixed. The effective stresses were calculated using the density of the material and had been taken as the initial stresses. FISH functions were developed to calculate the necessary MCC properties and to store the necessary histories.

The soil without the embankment was analyzed first to determine its initial state. This analysis was carried out under partially drained conditions. For this purpose a pseudo bulk modulus for the water was chosen as 30 Mpa (Wroth, 1979). Subsequent

computation involved the modeling of the peat and sand layers above the clay along with the construction of the initial embankment up to the level of 12.2 m. This was also carried out with the same partial drainage conditions as in the previous case. This portion of the embankment was modeled in four stages each with 2.6m height of fill material.

The embankment height was increased by 1.8m (6ft) . While the initial slope of the embankment was 1:2 (Vertical : Horizontal), the additional fill was added using a steeper slope of 1:1.2. This was carried out under a fully undrained condition, with the bulk modulus of the water of 2 Gpa (Wroth, 1979). There were field observations available with the additional 1.8m fill above 12.2m elevation. The results from the analysis were tabulated together with the observed values in Table 5.3.

Finally more layers of additional fill were added. Each layer had a thickness of 0.9m. The differential settlement of the crest of the embankment was calculated for each increment. Failure was assumed to occur when the differential settlements reached 150 mm (0.5 ft). The corresponding pore pressures at failure were calculated (Table 5.3). The table also shows the predicted values of previous analyses (McCarron and Chen, 1987, Wroth, 1979).

Fig. 5.5 shows the measured and predicted lateral displacement variation in two different locations. It can be seen from the tabulated values as well as Fig. 5.5 that the model computations provides a good representation of measured data.

Item Predicted	A	**B**	C	D	E
Additional horizontal movement due to 1.8 m of fill: (mm) at					
SI-3, Elev -9.1m	5-20	**11**	41	8.4	4.3-220
SI-3, Elev -21.3m	3-13	**2**	15	6.9	0.5-220
SI-4, Elev -9.1m	-5-5	**5**	18	5.3	6.3-135
SI-4, Elev -21.3m	0	**0**	0	0	0
Additional settlement of SP-1 due to 1.8m of fill: (mm)	17	**18**	66	21	19-348
Additional pore pressure due to 1.8m of fill: (meter head of water) at					
P-3	2.9	**2.9**	2.7	2.5	1.8-7.9
P-4	2.0	**2.5**	2.9	3.9	2.2-6.7
P-6	1.7	**1.5**	1.7	3.6	0.8-4.0
Additional heave due to 1.8m of fill: (mm) at					
H-1	-8-2	**-8**	0	2.5	0--122
H-2	-9-1	**-3**	0	1.8	0--157
Additional height of fill at failure: (m)	5.7	**5.4**	6.4	-	2.4-8.2
Additional pore pressure at failure: (meter head of water) at					
P-3	6.7	**5.9**	8.2	-	3.9-11.6
P-4	6.6	**5.1**	8.6	-	3.8-12.8
P-6	3.3	**3.4**	2.4	-	1.2-7.9
A – Observed Values, B-Present Computations, C-Wroth, D- McCarron and Chen, E-Symposium Predictions					

Table 5.3: Predicted and measured responses of the MIT symposium embankment

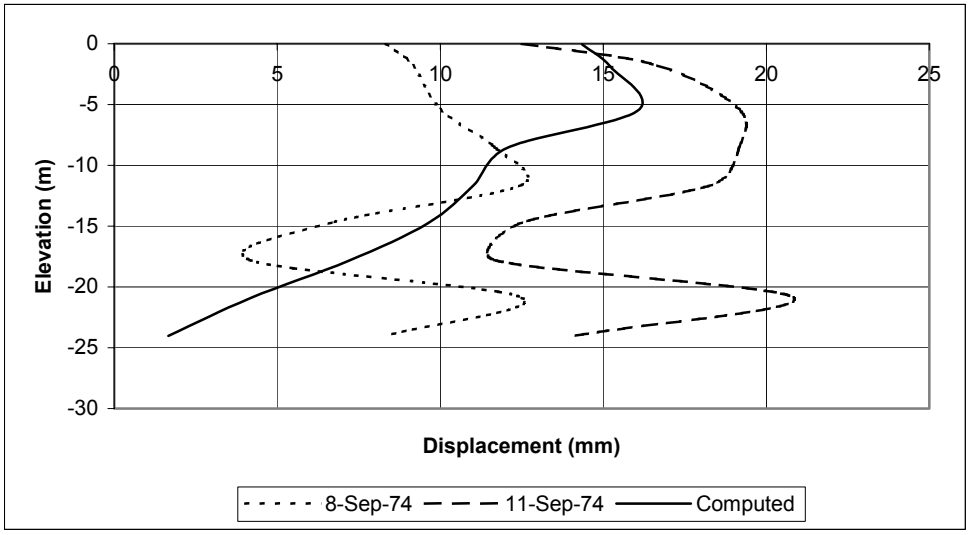

(a) SI - 3

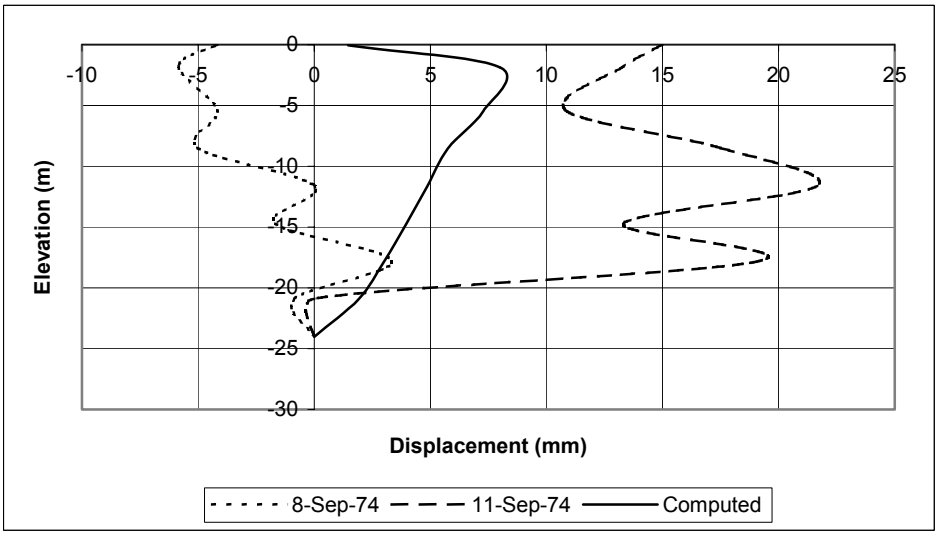

(b) SI - 4

Fig. 5.5: Lateral displacement variation of MIT symposium embankment (Field data from McCarron and Chen, 1987)

5.5 Embankment with stone columns

In order to study the effect of stone columns on the deformation of the embankment, the clay was reinforced with stone columns. It was, found, however, that the use of such inclusions led to only modest changes in the deformation pattern.

Therefore, it was decided to replace the Boston blue clay with a much weaker clay. The parameters used for this clay are as shown in Table 5.4. The properties of sand and fill layers were kept the same as used previously. In addition the peat layer was also removed. The modified arrangement used for such analysis is given in Fig. 5.6.

Parameter	Value
Shear Modulus, G (MPa)	1
Soil Constant, M	1.0
Slope of normal consolidation line, λ	0.15,0.10
Slope of elastic swelling line, κ	0.03
Reference Pressure, p'_1 (kPa)	1
Specific Volume at reference Pressure, υ_λ	2.3
Dry Density (Mg/m^3)	1.8
Porosity	0.5

Table 5.4: Soil properties of weaker clay

5.6 Modeling of sand columns

The sand columns were modeled using cylindrical meshes and were assumed to follow the Mohr–Coulomb constitutive behavior. The properties of the sand column

material used in the analysis are tabulated in Table 5.5. In general, the ATTACH command provided in FLAC 3D are used to join grids on different segments. However, since wedges were used in the embankment section, the use of the cylindrical mesh for the sand column created a problem with mesh disparity for direct use of the ATTACH command. Therefore, an interface was used to join the two grids in the embankment section.

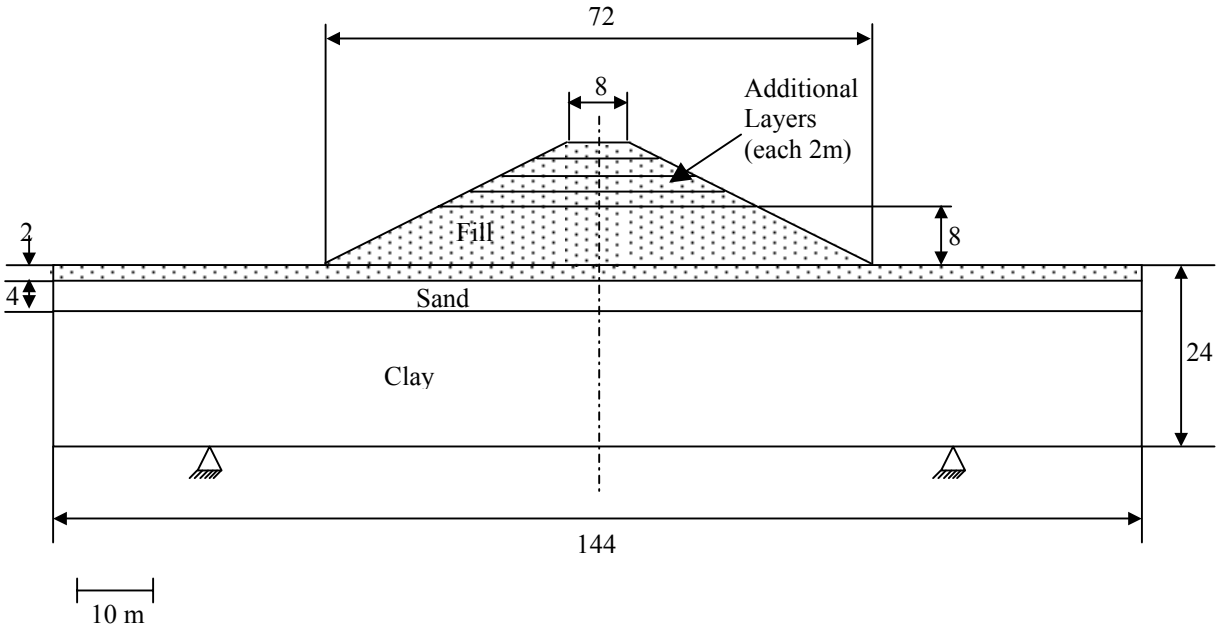

Fig. 5.6: Modified model used in the analysis (Dimensions are in m)

FLAC 3D represents interfaces as collections of triangular elements (interface elements), each of which is defined by three nodes (interface nodes). Interface elements can be created at any location in space. Generally, interface elements are attached to a zone surface face; two triangular interface elements are defined for every quadrilateral zone face. Interface nodes are then created automatically at every interface element, the contact is detected at the interface node, and is characterized by normal and shear

stiffness, and sliding properties. Each interface element distributes its area to its nodes in a weighted manner. Each interface node has an associated representative area. The entire interface is thus divided into active interface nodes representing the total area of the interface. Fig. 5.7 (b) shows the interface arrangement that was used between the columns and the embankment. The grid arrangements below (improved gound) and above (fill) the interface are shown in Fig. 5.7 (a) and (c) respectively.

Parameter	**Sand Column Material**
Bulk Modulus, K (MPa)	50
Shear Modulus, G (MPa)	10
Cohesion, C (kPa)	0
Internal Friction angle, ϕ (Deg)	32
Dilation angle, ψ (Deg)	0
Tensile strength, T (kPa)	1
Dry Density, γ (Mg/m^3)	2.0

Table 5.5: Soil properties of sand column material

The interface used to join different sub grids was assigned with a higher strength property with the INTERFACE command to prevent any slip or separation. FLAC 3D also requires the use of appropriate shear stiffness k_s and normal stiffness k_n; values of friction and cohesion were not needed. It was recommended that the k_n and k_s to be set to ten times the equivalent stiffness of the stiffest neighboring zone. The apparent stiffness (expressed in stress-per-distance units) of a zone in the normal direction is given by (FLAC 3D, 2002):

$$\max\left[\frac{\left(K+\frac{4}{3}G\right)}{\Delta Z_{min}}\right] \qquad (5\text{-}1)$$

where K and G are the bulk and shear moduli, of the material which has the lowest stiffness, respectively; and ΔZ_{min} is the smallest width of an adjoining zone in the normal direction.

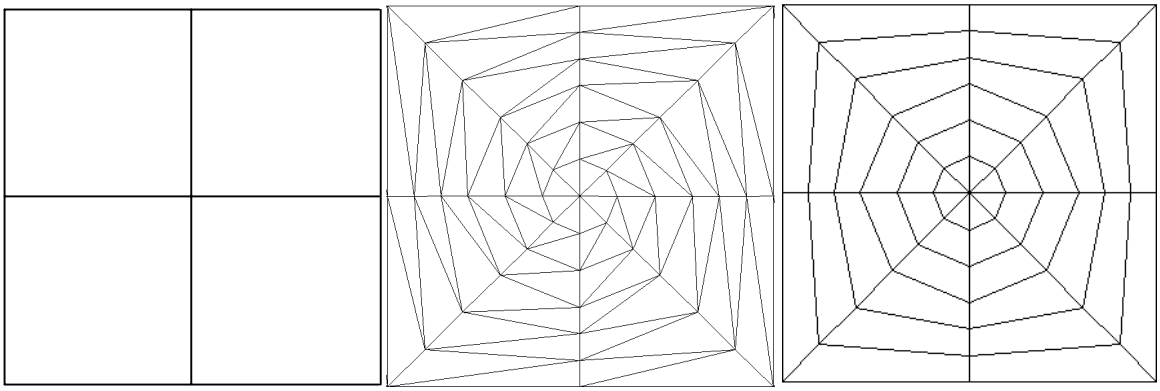

(a) Embankment (b) Interface (c) Improved ground

Fig. 5.7: Grid patterns of interface and vicinity.

The interface in this problem is used between the same material (fill) with different sub grids. Therefore, (K+4G/3) equals 43 Mpa. The minimum zone size adjacent to the interface is 2 m (Fig. 5.6). Thus, the shear stiffness and normal stiffness were chosen to be 430 x 10^6 / 2 – i.e., $k_n = k_s = 2.2 \times 10^5$ kPa/m.

5.7 Sand column performance

A number of points on a grid as shown in Fig. 5.8 were selected to observe the displacement variation with the different column improvement arrangements. These

points are identified with the row followed by the column number such as A1, A2, and so on.

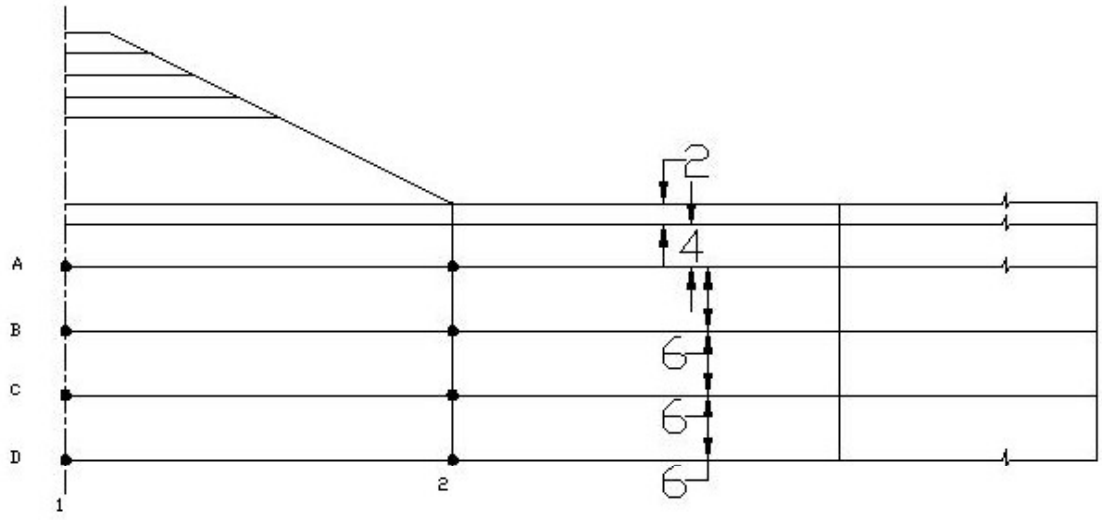

Fig. 5.8: Observation points

The weaker clay was improved with sand columns with a square grid arrangement. Sand columns in practice are constructed with diameters of 0.75 m to 1.5 m and the spacings of 1.8 m to 3.0 m. They usually result in approximately 20 to 35 % soil replacement (Bachus and Barksdale, 1989). In some cases it may go up to 50%. Accordingly, analyses were conducted on sand columns with diameter 1.4 m installed at a spacing of 2.4 m.

5.8 Stress Concentration

When the composite ground is loaded, studies have shown that a concentration of stress occurs within the granular pile accompanied by a reduction in stress in the less stiff surrounding clayey soil (Fig. 5.9) (Bergado et al., 1996). This is due to the approximately same vertical settlement of the granular material and the surrounding soil.

Stress concentrates on the column material because of its higher stiffness and causes a difference in vertical stress within the column and in the surrounding soil. Such a disparity or stress concentration is also evident from the results of the analysis present here (Fig. 5.10). The stress distribution is generally defined in terms of a stress concentration factor, n, as:

$$n = \frac{\sigma_c}{\sigma_s} \tag{5-1}$$

where σ_c is the stress in the column and σ_s is the stress in the surrounding soil.

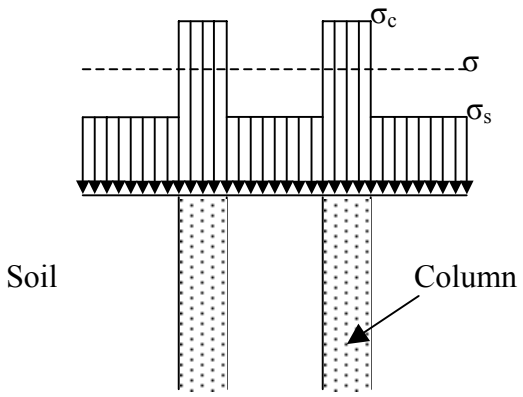

Fig. 5.9 Diagram of vertical stress distribution along column and surrounding soil

The magnitude of the stress concentration factor is depended on the modular ratio (E_c/E_s) and the improved area ratio, a (A_c/A_T Eq. 3-14). For a modular ratio of 10 and an improved area ratio of 27% the stress concentration factor was found to be 1.2. Reported values of the stress concentration factor were found to vary between 2.5 and 5.0 (e.g. Bergado et al., 1996, Barksdale, 1987). For rapid loading under undrained conditions such as the one here, however, stress concentration will not occur until sometime after the full loading has been applied (Bachus and Barksdale, 1989). Based on a full-scale test

embankment observation on soft clay with a low improved area ratio of 6%, Bergado et al., (1996) reported that the stress concentration factor decreased to 1.45 with increasing applied load. Consequently, with a higher improved area ratio of 27% as the one here the stress concentration factor may be even less. A stress concentration factor 2 is usually adopted in United States practice (Barksdale, 1987).

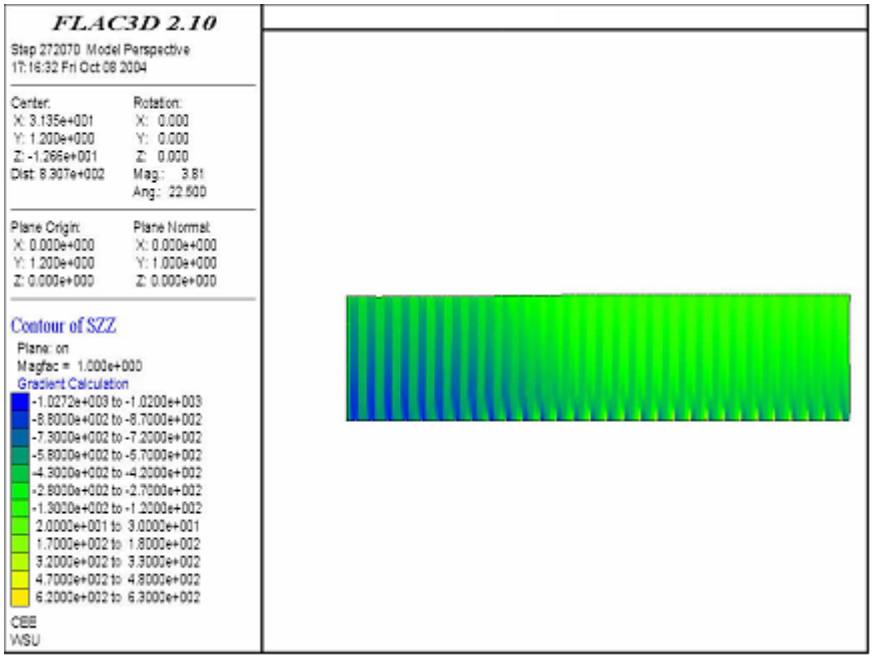

Fig. 5.10 Vertical stress distribution along column and surrounding soil from FLAC 3D

5.9 Area of improvement

The selection of the appropriate area is important for sand column improvement to be effective. Clearly, replacing the whole area of the weak soil with sand columns will have the maximum beneficial effect but it will be highly cost ineffective. This study considered different locations beneath the embankment for improvement and to compare their effectiveness.

Fig. 5.11 shows the typical locations of improvement considered. In the first arrangement, sand columns with a diameter of 1.4 m and 2.4 m spacing were placed in the clay underneath the embankment up to 36 m on either side of the embankment. This arrangement had columns up to 72 m from the centerline in both directions. The outer distance was reduced to 18 m in the second arrangement and as a result it had columns up to 54 m from the centerline in both directions. The third arrangement had columns only under the embankment, i.e. up to 36 m from the centerline in each direction. In the forth arrangement, columns were placed spanning half of the width of the area under the embankment, i.e. up to 18 m from the centerline in both directions. The fifth and sixth arrangements had no columns in the central 36 m of clay under the embankment. The former had columns placed from 18 m of the centerline and extended to 54 m in both directions while the latter 18 m from the centerline to 36 m in both directions. The summary of the arrangement is provided in Table 5.6. The reinforcement arrangements were modeled with Modified Cam- Clay behavior for the clay and Mohr–Coulomb behavior for the sand columns.

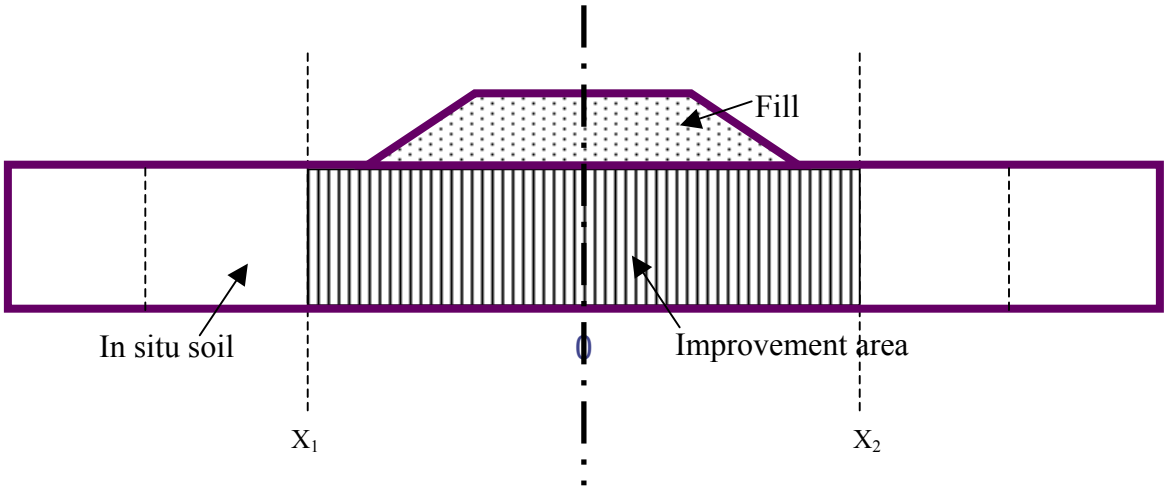

Fig. 5.11 A typical layout of improvement

The load on the embankment was increased incrementally by raising the height of the embankment every 2 m. The vertical displacement (the Z-displacement) was observed at A1 and the lateral displacement (the X-displacement) was observed at A2. The improvements in the displacement ratio (Displacement of improved ground / Displacement of in situ soil) are as shown in Fig. 5.12.

Arrangement	**X_1**	**X_2**
LO 1	-72	+72
LO 2	-54	+54
LO 3	-36	+36
LO 4	-18	+18
LO 5	-54 to -18	+18 to +54
LO 6	-36 to -18	+18 to +36

Table 5.6: Summary of the arrangements

It can be seen that while all arrangements result in an improvement in the displacement ratio, the amount is dependent on the type of arrangement. Layout 1 (LO 1) which had columns up to a distance of 72m in each direction from the centerline produced the best improvement. The displacement vectors of the unimproved ground under a typical height of embankment are as shown in Fig. 5.13. Note that though the loading is concentrated within the region of –36 m to +36 m, the vectors spread out for a longer distance from the centerline. Therefore, placement of sand columns up to where the vectors become small (such as LO 1 with-72 to +72 m) will be most effective. On the

other hand, LO 4 with columns at 18m in each direction with a lesser number of columns produces a comparative improvement in the displacement ratio.

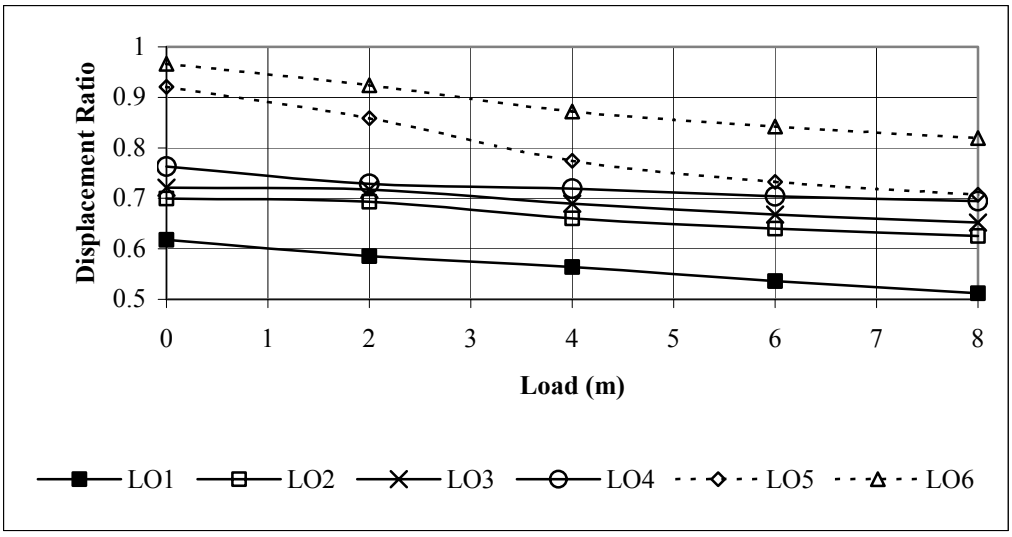

(a) Vertical displacement ratio at A1

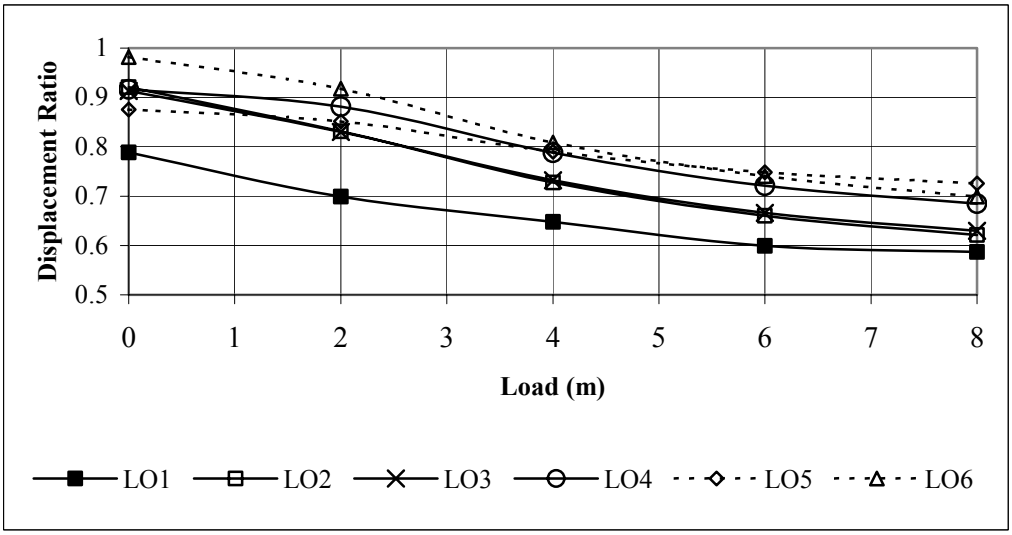

(b) Lateral displacement ratio at A2

Fig. 5.12: Displacement ratio for different arrangement of columns.

It is also interesting to note that LO 5 and LO 6 are effective only to reduce lateral displacements but not vertical displacements. Another significant observation from the

results is that the lateral displacement ratio approached a value of 0.6 at higher loads regardless of the type of arrangement.

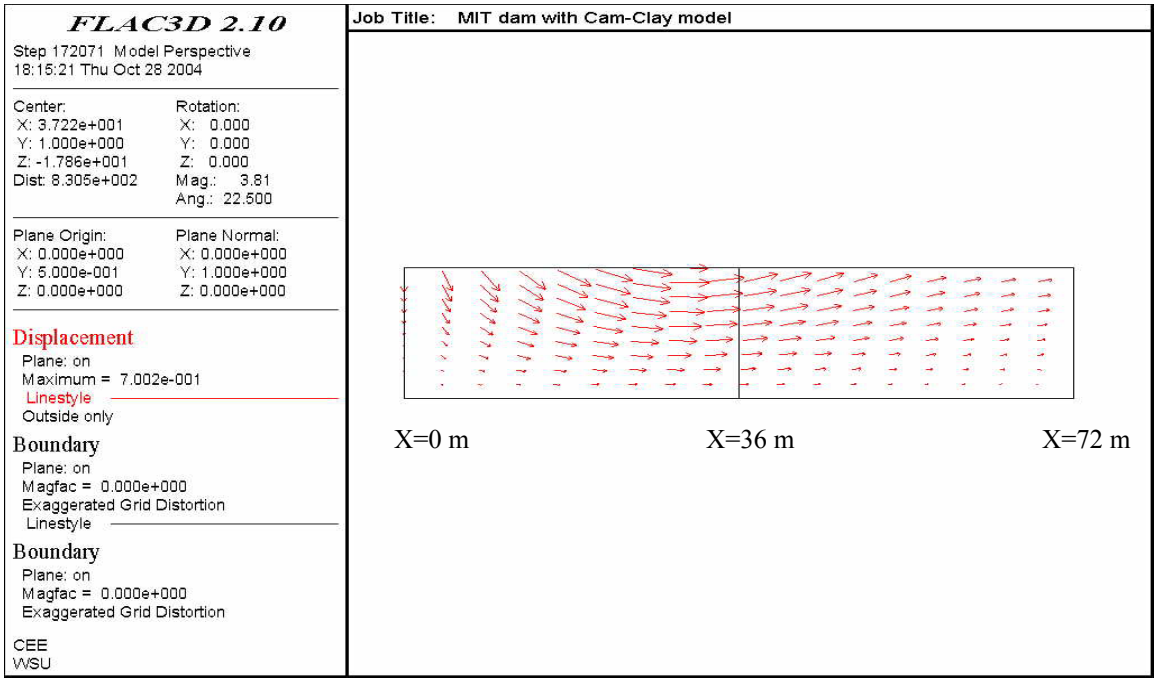

Fig. 5.13: Displacement vectors of the unimproved ground

5.10 Equivalent state based model

Since the improved ground consists of a mix of sand columns and in situ soil, following previous studies, it is possible to consider it as a composite medium with equivalent properties. Unlike the previous studies, which focused on elastic properties, the attention here is on the equivalent critical state properties.

The material properties for the equivalent model were calculated based on the critical state lines of individual constituents using Fig. 3.7. The critical specific volumes of the mixed soil at the mean effective pressure of 1 kPa were calculated based on the improved area (Eq. 3-26). The corresponding λ values were determined by assuming the critical state lines to pass through the Ω point (10300 kPa, 1.25). Such calculations

needed the pseudo bulk modulus of water for partially drained conditions. A trial and error approach was used to find its value. Analysis was first carried out with a chosen initial value of the bulk modulus for Arrangement 1. This value was adjusted until it produced results equal to the original set up. The calculated final pseduo bulk modulus for the partially drained conditions for the equivalent model was 30 Mpa.

The calculated equivalent properties using the procedure outlined in Chapter 3 for a typical case with 1.4 m diameter sand columns arranged with a spacing of 3.0 m are also shown in Table 5.7. Note that this arrangement resulted in an improved area ratio, a, of 17.1 % (Eq. 3.14).

Parameter	Column material	In situ soil	Mix soil
Shear Modulus, G, Mpa	10	1	2.54
Soil Constant, M	1.28	1	1.048
Slope of NCL line, λ	0.19	0.15	0.156
Slope of elastic swelling line, κ	0.04	0.03	0.032
Specific volume at p' of 1kPa	3.0	2.3	2.687
Dry density, Mg/m^3	2.0	1.8	1.834
Porosity	0.6	0.44	0.47

Table 5.7: Equivalent properties of the mix soil

Modified Cam- Clay model of FLAC 3D with equivalent properties was used in subsequent analyses of the arrangements. The water table was considered to be located on the ground surface. Vertical displacement ratios at location A1 and lateral

displacement ratio at A2 were compared. The different diameters of sand column and spacing considered in the analyses are shown in Table 5.8. Since the arrangements are symmetric with respect to the centerline of the embankment only half of the model was used in the analysis. The unit cell width of the column (i.e. spacing) was taken as the width of the model. The comparisons for Arrangement 2 are plotted in Fig. 5.14.

It can be seen from Fig. 5.14 that the results from the analysis using the actual arrangement and the equivalent model are almost identical with each other. The use of equivalent properties produced near identical results with their respective original analyses for other arrangements as well. In the above analysis the equivalent model uses parameters that are back calculated.

Arrangement	**Diameter/ (m)**	**Spacing/ (m)**	**λ of the in situ soil**
1	1.4	2.4	0.15
2	1.4	3.0	0.15
3	1.2	1.8	0.15
4	1.2	2.0	0.15
5	0.8	1.75	0.15
6	1.0	2.0	0.10

Table 5.8: Different column arrangements

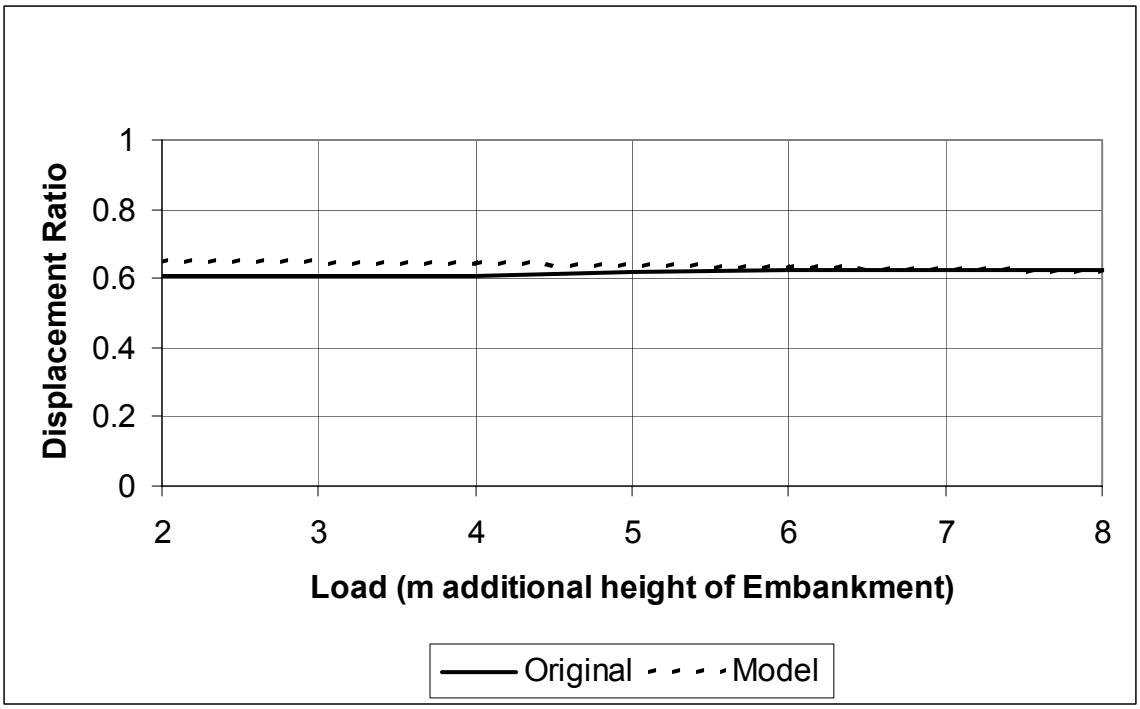

(a) Vertical displacement

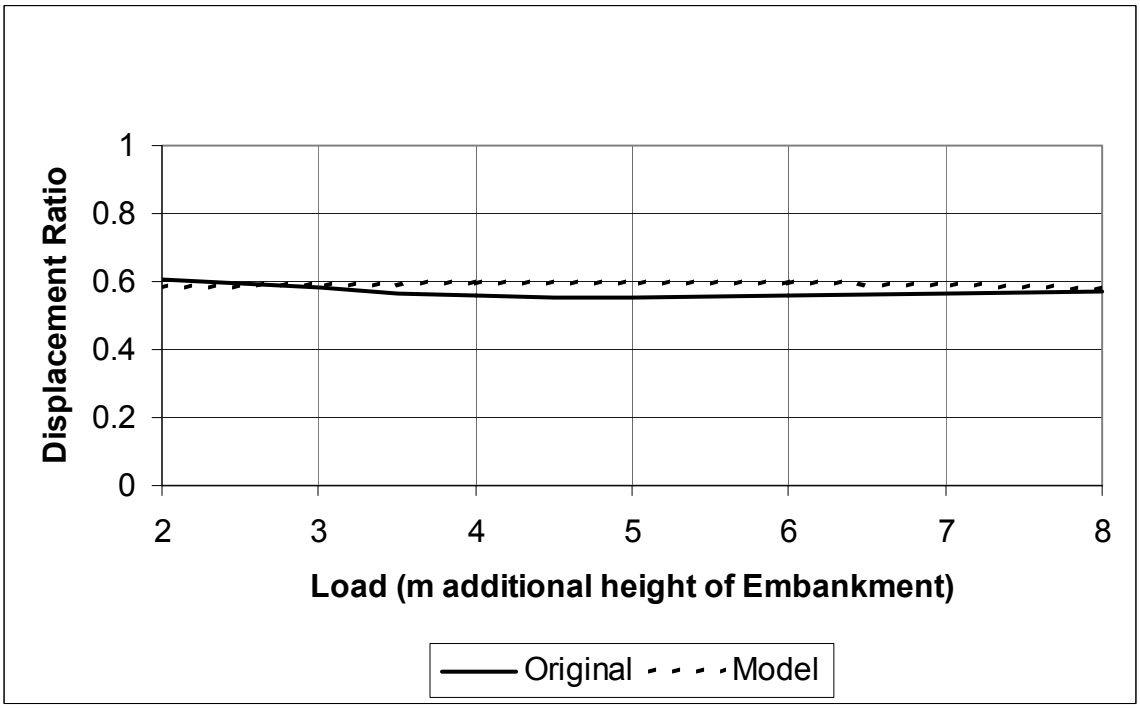

(b) Lateral displacement

Fig. 5.14: Comparison of the performance of original and equivalent model analysis. (diameter = 1.4 m, spacing = 3.0 m)

5.11 Parametric studies

The model with equivalent critical state properties was used to study the effects of modular ratio, improved area ratio and state parameter on the displacement patterns of various embankments. The effect of using partially penetrating sand columns on displacement pattern was also evaluated.

Aboshi and Suematsu (1985) have produced a summary of the effects of modular ratio, improved area ratio, angle of internal friction of the granular material and stress concentration factor on vertical (settlement) displacement ratio of embankments. They also made a comparison of the different methods of estimating the settlement reduction of improved ground. Bergado et al., (1987) have updated the observations of Aboshi and Suematsu (1985) using their own tests results on Soft Bangkok clay. The results are as shown in Fig. 5.15.

A numerical analysis on an embankment on Bangkok clay was carried out using the proposed equivalent model with the modular ratios of 10 and 20. The properties used for Soft Bangkok clay are tabulated in Table 5.9. It can be seen that the results for the proposed method compares well with measured data on a full-scale plate load test by Bergado et al., (1987) with a modular ratio of 16.7. It can also be seen that beyond a 40% replacement there is not much effect by sand columns on settlement reduction. Note also that some of the past methods report a displacement reduction ratio of zero. This means that no settlement occurs in the improved ground. This is not a realistic prediction of field behavior. As predicted by the current and some past analyses the settlement reduction with sand columns would approach and asymptotic non-zero value, depends on the modular ratio.

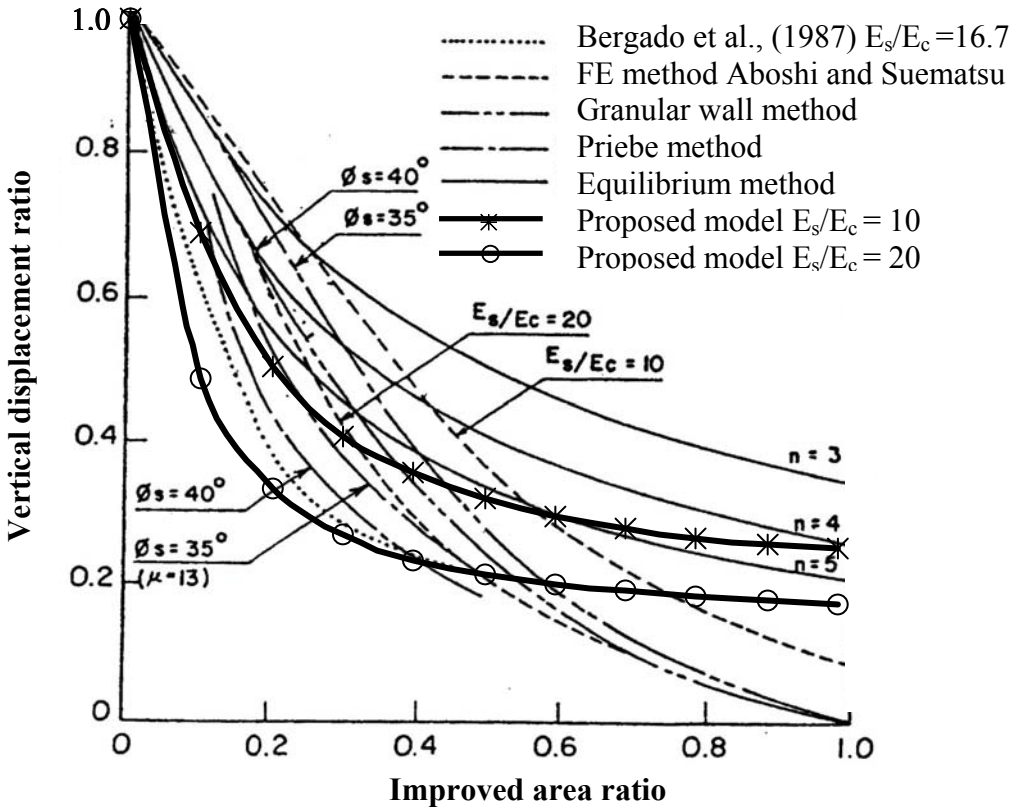

Fig. 5.15: Vertical displacement ratio with improved area ratio (Aboshi and Suematsu, 1985, Bergado et al.,1987)

5.11.1 Importance of state parameter

In order, to highlight the wider applicability of the model further studies were conducted on an embankment constructed on another saturated weak clay. This embankment was constructed on the Cubzac-les-Ponts clay found in France (Leroueil et al., 1990). The properties of this clay were well defined and are summarized in Table 5.10. The sand column material was kept the same as in the previous analyses

The cross section of the FLAC 3D model of the embankment problem is shown in Fig. 5.16. The coordinate system was chosen to have the x-axis along the surface of the in Cubzac-les-Ponts clay and the z-axis along the centerline as shown in Fig. 5.16. The

water surface was taken to be along Z = 0 m line. The depth of the clay layer was taken as 24 m.

PROPERTY	VALUE
Shear Modulus, G (MPa)	1
Soil Constant, M	1.2
Slope of normal consolidation line, λ	0.1
Slope of elastic swelling line, κ	0.03
Reference Pressure, p'_1 (kPa)	1
Specific Volume at reference Pressure, υ_λ	2.179
Dry Density (Mg/m^3)	1.7
Porosity	0.52

Table 5.9: Soil properties of soft Bangkok clay (Source: Bergado et al., (1996))

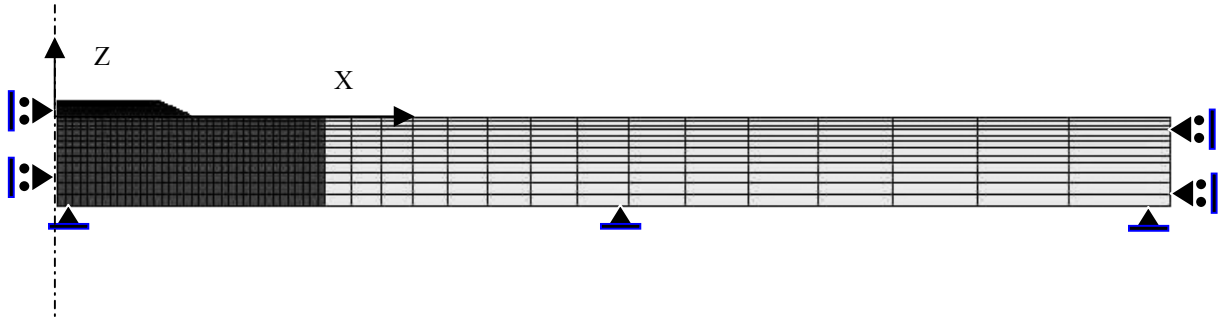

Fig. 5.16: Cross section of the model with boundary conditions

The analyses considered an improved area ratio variation from 0% to 100%. The modular ratios for the sand columns on soft clays have been found to vary between 10 and 40 (Balaam and Poulos 1978). Accordingly, modular ratios of 10, 20 and 30 were considered in the study. The equivalent λ values for the mix soil were estimated using

the critical state model as described earlier. Since different modular ratios were used, the corresponding κ values for the sand were calculated using (Britto and Gunn,1987):

$$K' = \frac{\upsilon p'}{\kappa} \tag{5-1}$$

where K′ is the effective bulk modulus, υ is the specific volume and p′ is the mean stress.

PROPERTY	VALUE
Shear Modulus, G (MPa)	1
Soil Constant, M	1.2
Slope of normal consolidation line, λ	0.13
Slope of elastic swelling line, κ	0.013
Reference Pressure, p'_1 (kPa)	1
Specific Volume at reference Pressure, υ_λ	2.45
Dry Density (Mg/m^3)	1.7
Porosity	0.52

Table 5.10: Soil properties of Cubzac-les-Ponts clay (Source: Leroueil.S at el, (1990)

The Cubzac-les-Ponts clay was loaded with an embankment of 4.5 m height. The vertical displacements were observed at different locations along the centerline (X = 0 m), and the lateral displacements were monitored at different depths along X = 36 m line. The variation of the vertical displacement ratio as a function of improved area ratio and state parameter for differing modular ratios are as shown in Figs. 5.17, 5.18 and 5.19, respectively. The effect of the state parameter can be clearly seen from the above plots.

Similar dependence on state parameter for the variation of lateral displacement ratios are shown in Figs. 5.20, 5.21, and 5.22.

Figs. 5.23 and 5.24 show the effect of the state parameter on improved performance for grounds with fixed values of modular ratios for vertical and lateral displacement ratios, respectively. It can be seen that the effect of the state parameter is much higher on the vertical displacement ratio than on the lateral displacement ratio. For example, an improved ground with area ratio of 30% and a modular ratio of 10 attains about 0.4 and 0.58 vertical displacement ratios, for state parameters of 0 and 20, respectively (Fig. 5.23). On the other hand, it attains about 0.36 and 0.38 in the lateral displacement ratios, for similar state parameters, respectively (Fig. 5.24).

The above figures can be used to determine the area ratio needed to improve a soil with given state parameter to achieve a particular displacement ratio.

5.11.2 Partially penetrating sand columns

In some cases, the stone columns do not penetrate the full depth of deep soil deposits. A set of analyses was performed to study the effect such partially penetrating columns on embankment settlement performance. The analyses considered full, half, and one-third depths of penetration. In addition, the effect of improving only half and one third width of the initial arrangement was also analyzed. Fig. 5.25 shows the pattern of such studies and Table 5.11 gives a summary of the variables used.

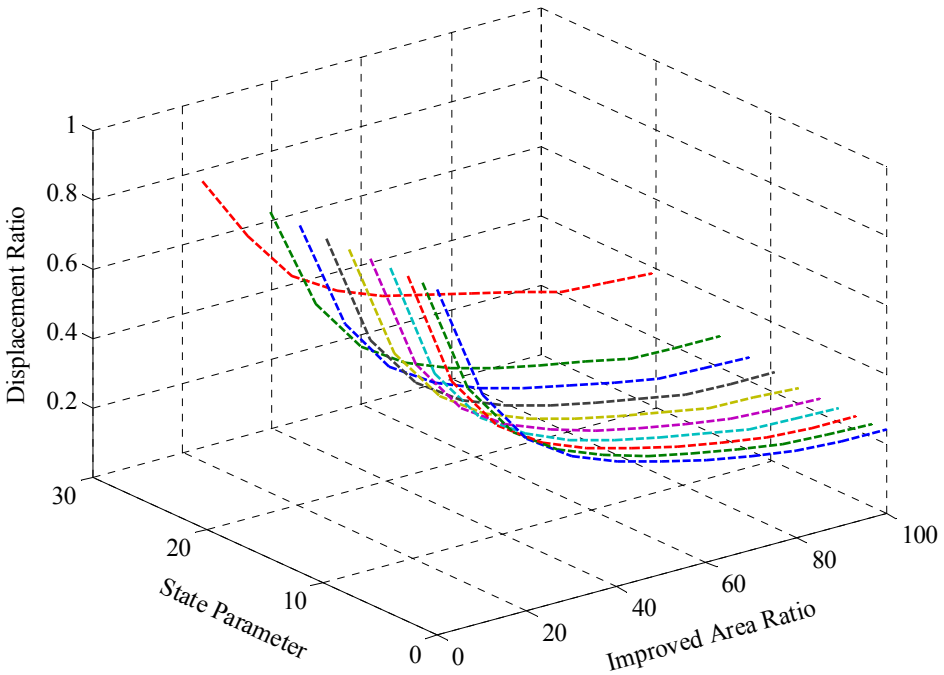

Fig. 5.17 The vertical displacement ratio in terms of state parameter and improved area ratio for the modular ratio of 10

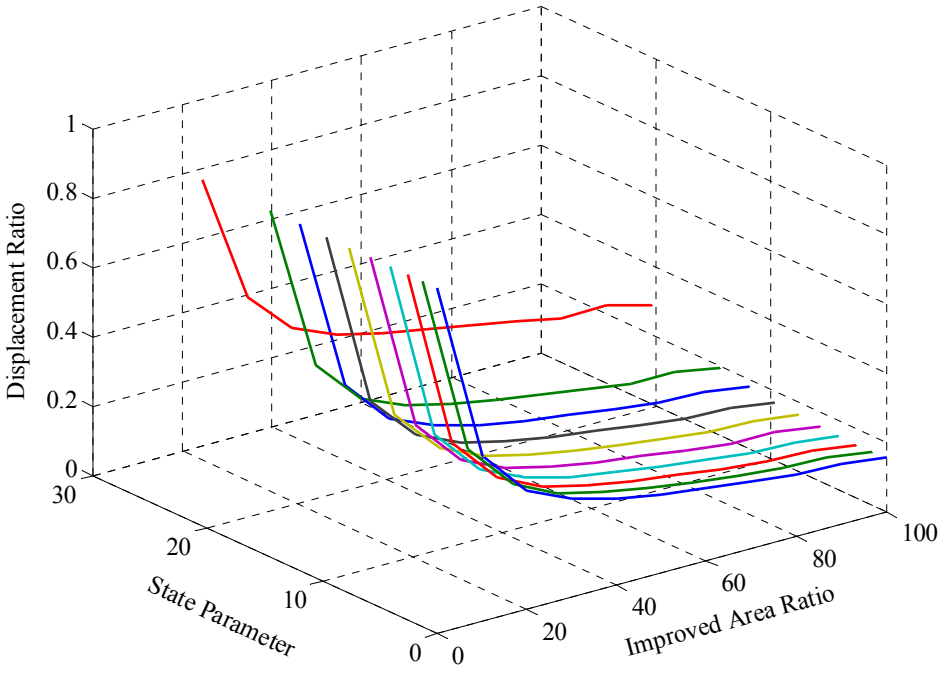

Fig. 5.18 The vertical displacement ratio in terms of state parameter and improved area ratio for the modular ratio of 20

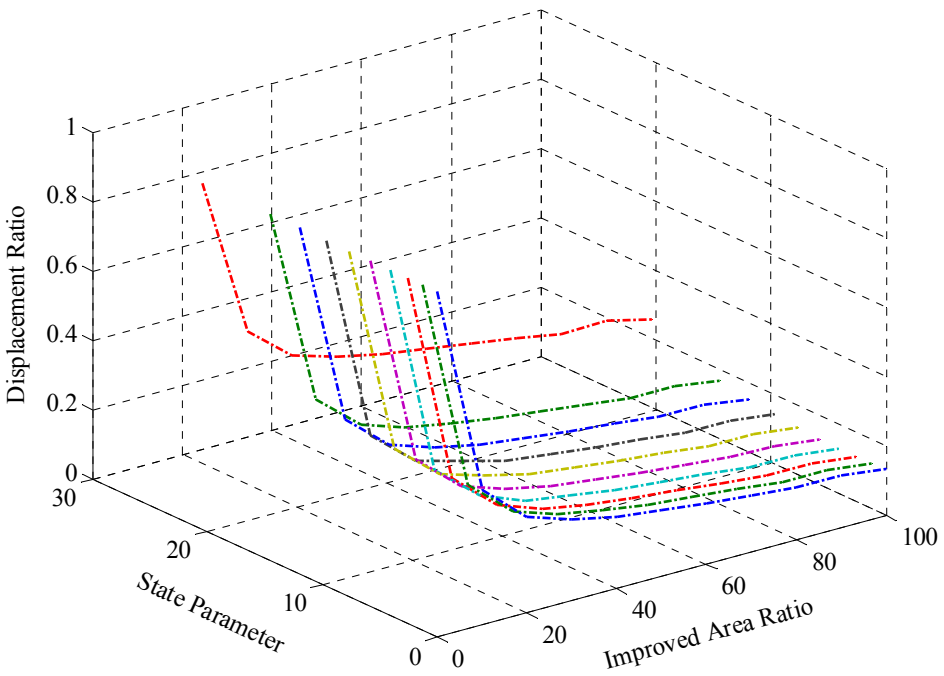

Fig. 5.19 The vertical displacement ratio in terms of state parameter and improved area ratio for the modular ratio of 30

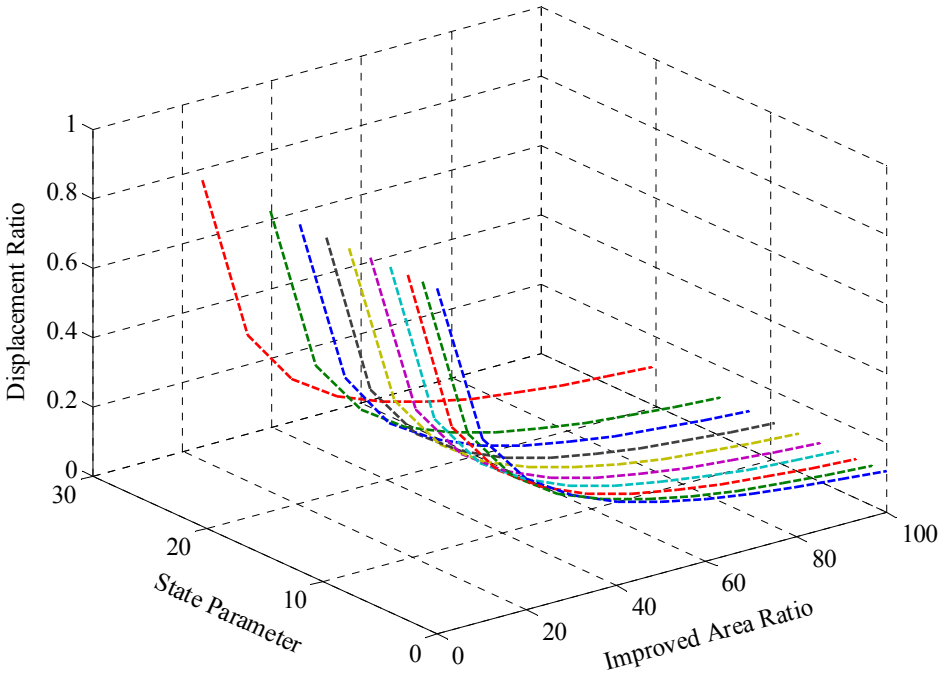

Fig. 5.20 The lateral displacement ratio in terms of state parameter and improved area ratio for the modular ratio of 10

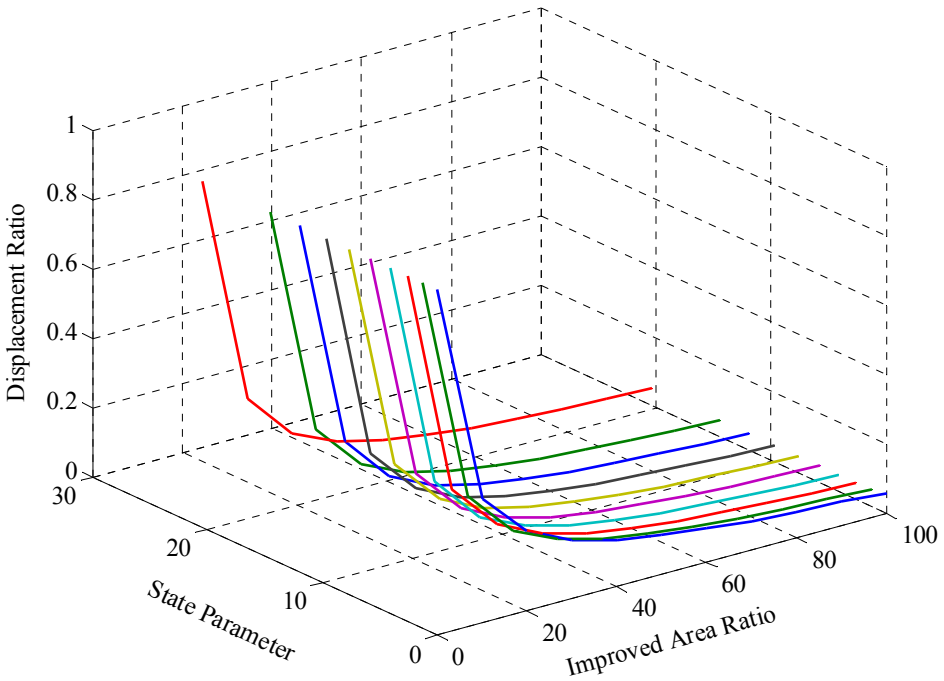

Fig. 5.21 The lateral displacement ratio in terms of state parameter and improved area ratio for the modular ratio of 20

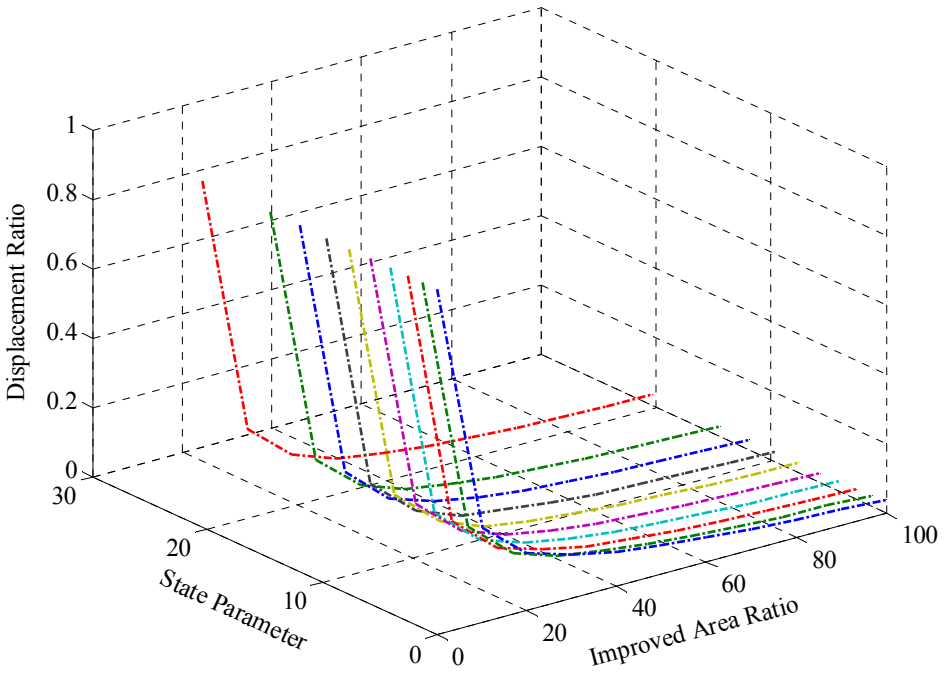

Fig. 5.22 The lateral displacement ratio in terms of state parameter and improved area ratio for the modular ratio of 30

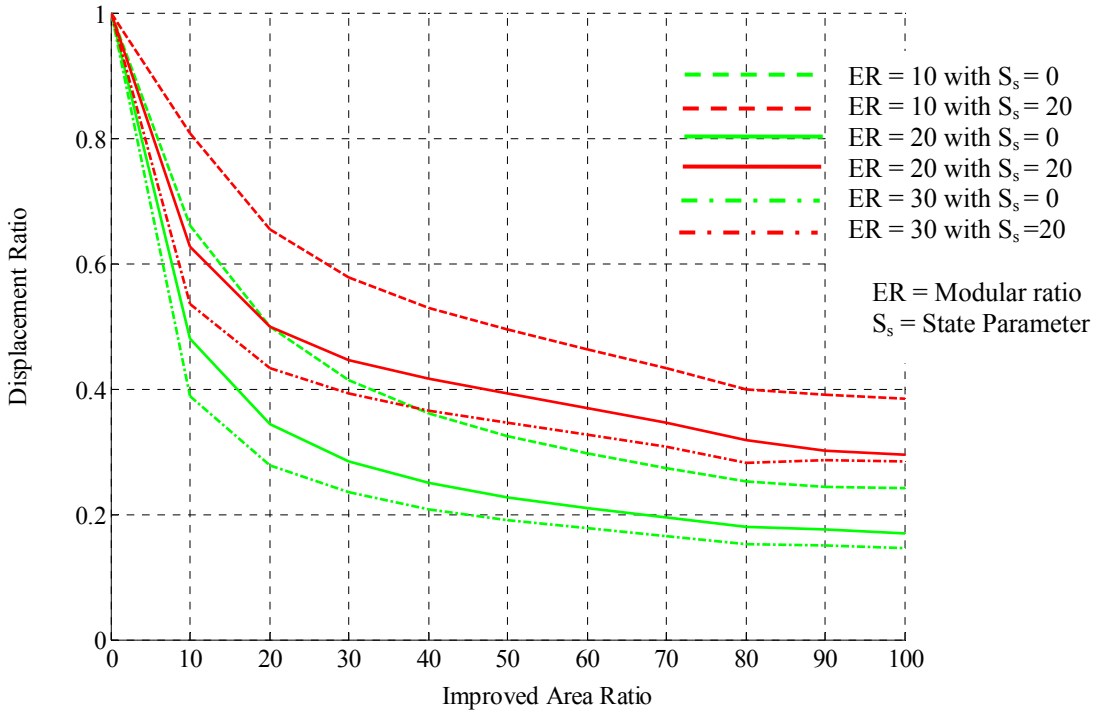

Fig. 5.23 The vertical displacement ratio in terms of state parameter and improved area ratio

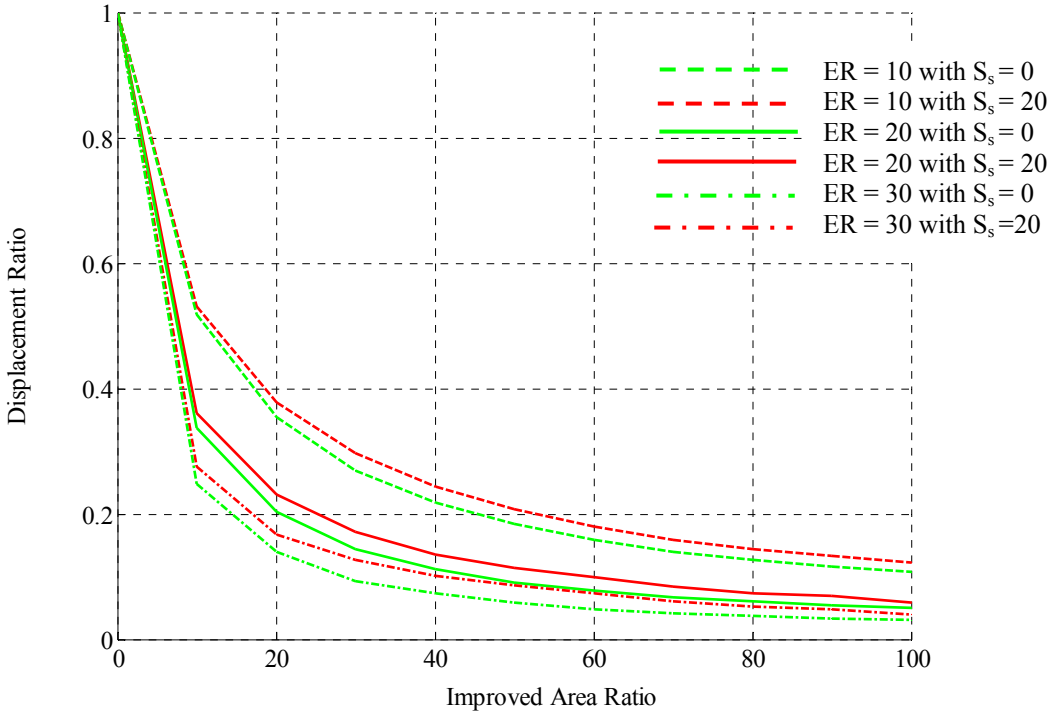

Fig. 5.24 The lateral displacement ratio in terms of state parameter and improved area ratio

The variations of lateral and vertical displacement ratio with the improved area ratio for the different patterns are shown in Fig. 5.26. It can be seen that partially embedded sand columns are effective for the improvement of lateral displacement ratio but not for vertical displacement ratio.

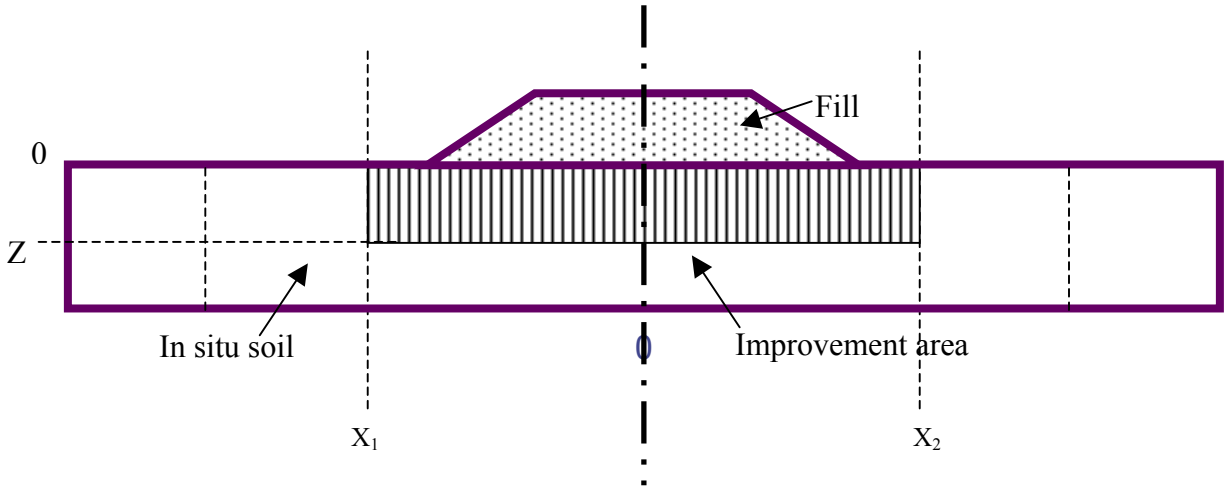

Fig. 5.25: Schematic diagram of the pattern of partial penetration improvement

PATTERN	X_1	X_2	Z
1	-72	+72	-24
2	-72	+72	-12
3	-72	+72	-8
4	-36	+36	-24
5	-18	+18	-24

Table 5.11: Summary of the patterns.

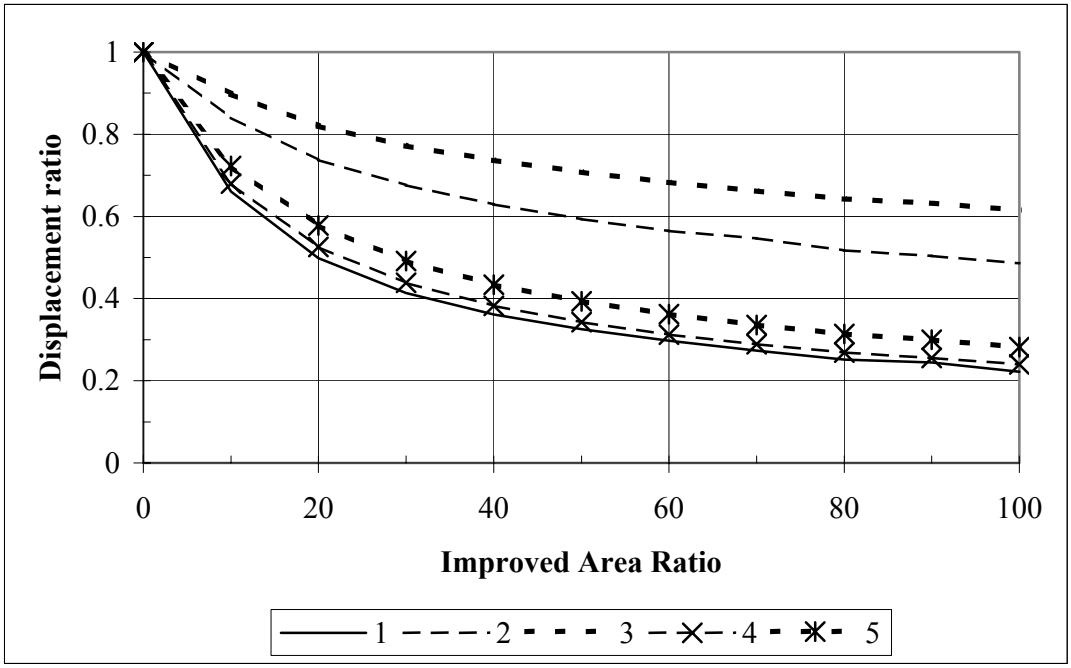

(a) Vertical displacement

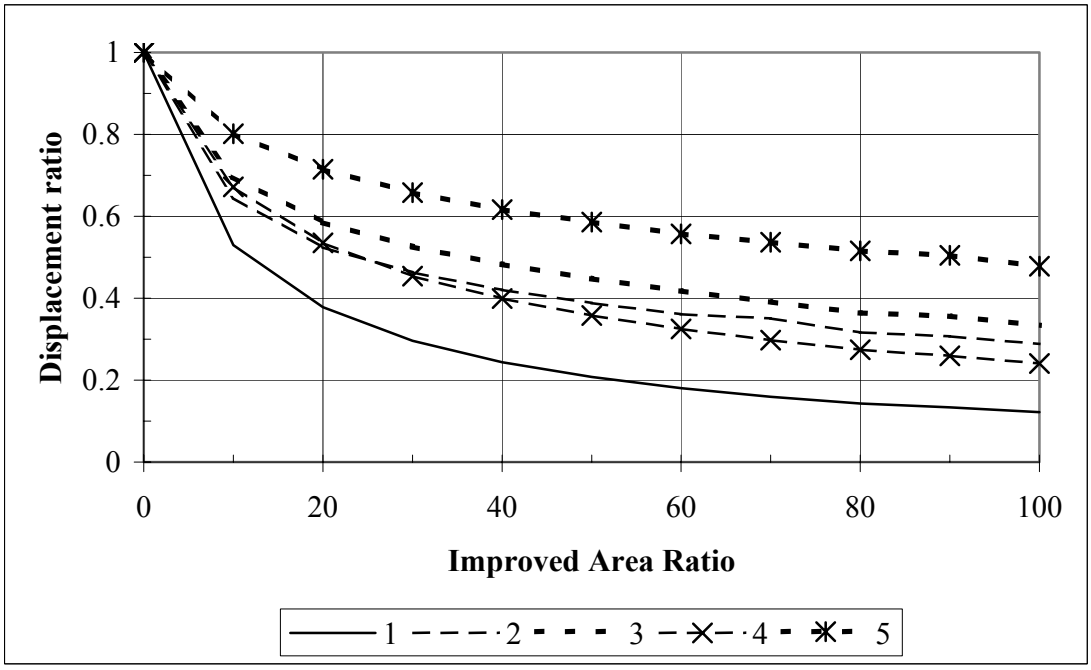

(b) Lateral displacement

Fig. 5.26 The variation of displacement ratio with improved area ratio for different reinforcement patterns

CHAPTER 6

CONCLUSIONS AND RECOMMENDATIONS

6.1 Conclusions

This study presented a numerical analysis of the field problem involving sand columns installed on weak soils. The analysis is based on the finite difference code FLAC 3D. The main focus of the study was on quantifying the effects of the state of soils on the performance of improved ground. A new method to quantify the equivalent state properties of improved ground using the properties of the constituent materials was developed. It made use of the fact that the critical state lines of most soils have a common origin at the Ω point.

The concepts developed here were applied to the displacement problem of an embankment constructed on weak soils. The performance of a field-instrumented embankment was used to verify the FLAC 3D model and its boundary conditions. The weak soil carrying the embankment was improved with sand columns of differing diameter and spacing and its response to applied loading was studied. The layout and extent of the improvement were also varied to study this effectiveness.

The analyses of the original arrangements as well those using equivalent state properties of the improved ground yielded nearly identical results. Consequently, use of equivalent state properties is an effective way to capture the performance of sand columns in weak soils. This is useful for practice as it saves on computing time.

The equivalent state properties were used to study the influence of initial state, modular ratio, layout and extent of reinforcement, and the use of partially penetrating

sand columns on the performance of improved ground. Based on these studies, the following conclusions can be drawn:

i) the state of soils plays an important role in influencing the displacement pattern of embankments in weak soils. The method presented here can quantify such influences (Figs. 5.17, 5.18, 5.19, 5.20, 5.21, 5.22, 5.23 and 5.24).

ii) the effectiveness of improvement is dependent on the layout and the extent of the reinforcement. Therefore, it is necessary to first perform a numerical analysis of the unimproved ground to determine the displacement patterns and then place sand columns for them to be effective in mitigating them.

iii) very little displacement improvement is registered beyond an improved area ratio of 40%.

iv) partially penetrating sand columns are effective to improve the lateral displacements embankments. They are not effective for controlling vertical displacements.

6.2 Recommendations

Although the concepts and the numerical models are used here for the analysis of the embankment problem, they are general enough for application to other problems in geotechnical engineering. It is recommended to extend the study to loose sands and other soft soils.

Few field studies are available on sand columns in soft soils for conditions other than embankments. Such studies are needed to verify further the numerical model. This

study ignored the time effects on the settlement behavior and it may be included in a future analysis. Sand columns have proven to be useful in providing drainage and reducing the potential for buildup of excess pore water pressure (Ashford et al, 2000) especially under earthquake loading. The numerical model could be extended to study the performance of the sand columns in reducing pore pressures under seismic loading.

REFERENCES

Aboshi, H., and Suematsu, N., (1985), Sand compaction pile method: State-of-the-Art paper, Proceedings 3rd International Geotechnical seminar on soil improvement methods, Nanyang Technical Institute, Singapore.

Aiban, S.A., (2002), Effectiveness of stone columns: field assessment, Geotechnical special publication 116, 1187-1199.

Alamgir, M., Miura, N., Poorooshasb, H.B., and Madhav, M.R., (1996), Computer and Geotechnics, 18 (4), 267-290.

Ashford, S.A., Rollins, K.M. Case Bradford, V.S., Weaver, T.J., and Baez, J.I., (2000), Liquefaction Mitigation using stone columns around deep foundations: Full Scale test results, Transportation Research record, 1736, 110-118.

Atkinson, J.H., (1993), An introduction to the mechanics of soils and foundations, McGraw-Hill, London.

Bachus, R.C., Barksdale, R.D. (1989), Design methodology for foundations on stone columns, Foundation engineering current principles and practice, 244-257.

Balaam, N.P., and Poulos, H.G., (1983), The behaviour of foundations supported by clay stabilised by stone columns, In: Improvement of ground; Proceedings of the Eighth European conference on soil mechanics and foundation engineering organized by the Finnish Geotechnical Society, 1, 199-204.

Barksdale, R.D., (1987), State of the art for design and construction of sand compaction piles, Technical report - US army engineer waterways experiment station.

Been, K., and Jefferies, M.G., (1985), A state parameter for sands, Geotechnique, 35 (2), 99-112.

Bergado, D.T., Anderson, L.R., Miura, N., and Balasubramaniam, A.S., (1996), Soft ground improvement in lowland and other environments, ASCE Press, USA, 186-232.

Bergado, D.T., Huat, S.H., and Kalvade, S., (1987), Improvement of soft Bangkok clay using granular piles in subsiding environment, Proceedings of 5th International Geotechnical seminar on case histories in soft clay, Singapore, 219-226.

Britto, A.M., and Gunn, M.J., Critical state soil mechanics via finite elements, Ellis Horwood.

D'Appolonia, D.J., Lambe, T.W., and Poulos, H.G., (1971), Evaluation of pore-pressures beneath an embankment, Journal of the soil mechanics and foundation division, ASCE, 97, SM6, 881-897.

Drucker, D.C., and Prager, W., (1952), Soil mechanics and plasticity analysis or limit design, Q. Appl. Math., 10(2), 157-165.

Eshelby, J.D., (1957), The determination of the elastic field of an ellipsoidal inclusion and related problems, Proceedings of the Royal Society, London, A (241), 376-396.

FLAC 3D, (2002) Fast lagrangian analysis of continua in 3 dimensions, Version 2.1, Itasca consulting group, Inc., Minnesota.

Huang, T., and Chen, W., (1990), Simple procedure for determining cap – plasticity – model parameters, Journal of geotechnical engineering, 116 (3), 492-513.

Kirsch, F., and Sondermann, W., (2003), Filed measurements and numerical analysis of the stress distribution below stone column supported embankments and their stability, Proceedings of the international workshop on geotechnics of soft soils – Theory and practice.

Klotz, E.U., and Coop, M.R., (2001), An investigation of the effect of soil state on the capacity of driven piles in sands, Geotechnique, 51 (9), 733-751.

Ladd, C.C., Whittle, A.J., and Legaspi, Jr., D.E., (1994), Stress-deformation behavior of an embankment on Boston blue clay, Vertical and horizontal deformation of foundations and embankments: Proceedings of settlement, 1730-1759.

Lambe, T.W., (1973), Predictions in soil engineering, Geotechnique, 23, 149-202.

Lambe, T.W., D'Appolonia, D.J., Karlsrud, K., and Kirby, R.C., (1972), The performance of the foundation under a high embankment, Journal of Boston Society of Civil Engineering, 59.

Lawrence, D.M., (1980), Some properties associated with Kaolinite soils, Ph. D. Thesis, Gonville and Caius College, Cambridge University, Cambridge, UK.

Leroueil, S., Magnan, J., and Tavenas, F., (1990), Embankment of soft clays, Ellis Horwood.

McCarron, W.O., and Chen, W.F., (1987), A capped plasticity model applied to Boston blue clay, Canadian Geotechnical Journal, 24, 630-644.

Mitchell, J.K., (1981), Soil improvement – State of the art report, Proceedings from the international conference Soil mechanics, Foundation engineering, Stockholm, 4, 509-560.

Muhunthan, B., and Schofield, A. N., (2000), Liquefaction and dam failures, Proceedings of ASCE GeoDenver 2000, Geotechnical Special Publication (101), 266-280.

Omine, K., and Bolton, M.D., (1998) Application of homogenization method to improved ground with cement-treated soil columns, Technical report - Department of Engineering, Cambridge University.

MIT,(1969), Performance of an embankment on clay, Interstate-95, R69-67, Department of Civil Engineering, Massachusetts Institute of technology, Cambridge, Massachusetts.

Pillai, V.S., and Muhunthan, B. (2001), A review of the influence of initial static shear (K_α) and confining stress (K_σ) on failure mechanisms and earthquake liquefaction of soils. Paper No. 1.51, Proc. 4th International Conference on Recent Advances in Geotechnical Earthquake Engineering and Soil Dynamics, San Diego, California.

Pillai, V. S., and Muhunthan, B. (2002), Discussion of An investigation of the effect of soil state on the capacity of driven piles in sands, by Klotz, E.U. and Coop, M.R., Geotechnique, 52(8), 620-621.

Poorooshasb, H.B., and Meyerhof, G.G., (1996), Analysis of behavior of stone columns and lime columns, Computers and Geotechnics, 20(1), 47-70.

Priebe, H., (1976), Abschactzung des setzungsverhaltns eiens durch stopfverdichtung verbesserten baugrundees Die Bautechnik, 54, 160-162.

Priebe, H.J., (1995), The design of Vibro replacement, Ground engineering, 31-37.

Roscoe K.H., and Burland, J.B., (1968), On the generalised stress – strain behavior of 'Wet clay', Engineering Plasticity, Cambridge University Press, Cambridge, UK, 535-609.

Schofield, A., and Wroth, P., (1968), Critical state soil mechanics, McGraw-Hill, London.

Wang, J.G., Leung, C.F., and Ichikawa, Y., (2002), A simplified homogenization method for composite soils, Computers and Geotechnics, 29, 477-500.

Wood, D.M., (1990), Soil behaviour and critical state soil mechanics, Cambridge University Press, Cambridge, UK.

Wroth, C.P., (1979), The predicted performance of soft clay under a trial embankment loading based on the cam-clay model, Finite elements in Geomechanics, John Wiley and Sons, 191-208.